DOI: 10.24850/j-tyca-2025-04-04

Articles

Study of teleconnection between hydrological variables and climatological variables in a headwater basin of the Maipo River for forecast model application

Estudio de teleconexión entre variables hidrológicas y climatológicas en una cuenca de cabecera del río Maipo para la aplicación de modelos de pronóstico

Javiera Montalva[1], ORCID: https://orcid.org/0009-0005-4781-1534

Álvaro Ossandón[2], ORCID: https://orcid.org/0000-0003-2165-8736

Lina Castro[3], ORCID: https://orcid.org/0000-0002-9260-0307

[1]Departamento de Obras Civiles, Universidad Técnica Federico Santa María, Santiago, Chile, jmontalvameza@gmail.com

[2]Departamento de Obras Civiles, Universidad Técnica Federico Santa María, Valparaíso, Chile, alvaro.ossandon@usm.cl

[3]Departamento de Obras Civiles, Universidad Técnica Federico Santa María, Santiago, Chile, lina.castro@usm.cl

Corresponding author: Álvaro Ossandón, alvaro.ossandon@usm.cl

Abstract

This study conducts a teleconnection analysis of the seasonal streamflow during the dry season (winter and summer) at the Olivares River basin, a headwater of the Maipo River basin, with traditional climate indices (Antarctic Oscillation, Niño1+2, and Niño3.4), new indices obtained from sea surface temperature (SST) anomaly spatial fields, and in situ hydrometeorological variables from the previous season to identify potential predictors for implementing seasonal streamflow forecast models in the study area. To illustrate the potential of the predictors identified, we fit multiple linear regression models (MLRM) for seasonal streamflow forecast for 0- and 3-month lead times. The forecasts are validated using the leave-1-year-out cross-validation (LOOCV) approach and performance metrics such as the Pearson correlation coefficient (R), BIAS, Nash-Sutcliffe efficiency (NSE), and continuous rank probability skill score (CRPSS). Results show a good performance of the forecast model for cross-validation with R and NSE values ranging from 0.55 to 0.95 and from 0.28 to 0.88 for 0- and 3-month lead times during the dry season. This early implementation provides good perspectives for implementing probabilistic seasonal streamflow forecasting models, which can provide a powerful output to develop robust water management strategies to tackle water scarcity in the study area.

Keywords: Climate teleconnection, hydrometeorological variables, seasonal streamflow forecast, multiple linear regression model.

Resumen

En este estudio se realiza un análisis de teleconexión del caudal estacional durante la temporada seca (primavera y verano) de la cuenca del río Olivares, una cuenca de cabecera del río Maipo, con índices climáticos tradicionales (Oscilación Antártica, Niño1+2 y Niño3.4), nuevos índices obtenidos de campos espaciales de anomalías de temperatura de la superficie del mar (TSM) y variables hidrometeorológicas in situ de la temporada anterior con el fin de identificar potenciales predictores para la implementación de modelos de pronóstico de caudales estacionales en la zona de estudio. Para ilustrar el potencial de los predictores identificados, se ajusta modelo de regresión lineal múltiple para el pronóstico de caudal estacional para periodos de previsión de 0 y 3 meses. Los pronósticos se validan utilizando el enfoque de validación cruzada "leave-1-year-out cross-validation" (LOOCV) y métricas estadísticas tales como el coeficiente de correlación de Pearson (R), sesgo porcentual (BIAS), coeficiente de eficiencia de Nash-Sutcliffe (NSE), y *continuous rank probability skill score* (CRPSS). Los resultados muestran un buen desempeño del modelo de pronóstico para la validación cruzada con valores de R y NSE que oscilan entre 0.55 y 0.95, y entre 0.28 y 0.88 para un tiempo de pronóstico de 0 y 3 meses durante la temporada seca. El modelo implementado brinda una buena perspectiva para la implementación de modelos probabilísticos de pronóstico de caudales estacionales, lo que puede resultar en una herramienta útil para el desarrollo de estrategias sólidas de gestión del recurso hídrico durante el periodo de escasez hídrica en la zona de estudio.

Palabras clave: teleconexión climática, variables hidrometeorológicas, pronóstico de caudal estacional, modelos de regresión lineal múltiple.

Received: 18/01/2023

Accepted: 31/05/2024

Published *ahead of print*: 10/06/2024

Version of record: 01/07/2025

Introduction

Seasonal streamflow forecast (SSF) has the potential to underpin the long-term management and planning of water resources. For instance, it can be used to make strategic allocations for key sectors such as water supply, irrigation, hydropower generation, industry, mining operations, and navigation (Araya *et al.*, 2023); to create flood mitigation strategies (Paiva *et al*., 2013; Kompor, Yoshikawa, & Kanae, 2020); and as a drought management tool (Chiew, Zhou, & McMahon, 2003; Sutanto, Wetterhall, & Van Lanen, 2020; Sutanto & Van Lanen, 2021). In several regions worldwide, vulnerable to water stress linked with the heightened intensity of the water cycle, adopting proactive water management has become essential (Mendoza *et al.*, 2017). This need has been intensified in recent years due to the evident global impact of climate change (Winsemius *et al*., 2016; IPCC, 2022). These impacts are especially evident in Chile, which has experienced a significant rainfall deficit during the last decade (Garreaud *et al.*, 2017; Garreaud *et al.*, 2020) and an increase in the frequency of extreme events such as droughts and floods (Vicuña *et al*., 2013; González-Reyes, 2016; Wilcox *et al*., 2016; Serrano-Notivoli *et al*., 2021). Therefore, producing skillful SSF to support water

supply operations and planning has been a long-lasting task for the operational hydrology community; however, it is challenging due to the multiple error sources involved, such as predicting and forcing data errors, model structure selection, and model parameter errors (Mendoza *et al.*, 2017).

In Chile, SSF is employed for agricultural irrigation and hydropower generation during the spring-summer (September-March) season. The current operational SSF for the irrigation season is conducted by the Chilean Water Directorate (Dirección General de Aguas, DGA). This forecast is limited to a single lead time, released on September 1 at the season's outset. It relies on statistical models that correlate streamflow volumes with on-site measurements of hydrometeorological variables from the previous season, including precipitation, temperature, and snow water equivalent, among other variables (DGA, 2022). For hydropower generation, the SSF is conducted by the National Electrical Coordinator of the Central Interconnected System (CDEC-SIC) and follows a methodology similar to DGA. This approach relies on a statistical regression that utilizes in situ hydrometeorological information up to August (CONIC-BF, 2023). While these forecasts have been relatively reliable using only local historical information, the evident effects of climate change, such as the increased frequency and magnitude of extreme events and the need for forecasts with longer lead times to enhance water resource management (available before September 1), make it necessary to explore new forecasting methodologies.

Methods for seasonal streamflow forecasting are divided into dynamical, statistical, or hybrid approaches (a combination of dynamical and statistical models) (Block & Rajagopalan, 2009; Yuan *et al.*, 2015).

Dynamical methods employ hydrological simulation models to represent hydrological processes and generate initial hydrological conditions (IHC). Then, these models are forced with either historical meteorology or inputs derived from seasonal climate forecasts (Araya *et al.*, 2023; Bradley, Habib, & Schwartz, 2015; Petry *et al.*, 2023; Wood, Kumar, & Lettenmaier, 2005). Dynamical models for SSF have been implemented in Africa (Block & Rajagopalan, 2009; Bradley *et al.*, 2015; Wijayarathne & Coulibaly, 2020), Europe (Ćeron et al., 2010; Singla *et al.*, 2012; Arnal *et al.*, 2018), Australia (Bennett *et al.*, 2016), North America (Clark & Hay, 2004; Wood et al., 2005; Wijayarathne & Coulibaly, 2020) and South America (Araya *et al.*, 2023; Petry *et al.*, 2023). Araya *et al.* (2023) applied three conceptual rainfall-runoff models forced with historical meteorology ensembles to generate probabilistic SSF in Chile. They tested 12 different objective functions (OF) to calibrate and assess the skill of retrospective SSF in 22 catchments along the semiarid Andes Cordillera (28-37°S) for various lead times. Their findings revealed that hydrological consistency does not necessarily imply satisfactory SSF. However, using an OF that allows low and high flows to be considered simultaneously provides a reasonable balance between hydrological consistency and forecast performance. In the case of statistical approaches, they focus on identifying the empirical relationship between seasonal streamflow and large-scale climate variables and/or in situ watershed observations. Statistical approaches span from multiple linear regression (MLR) (Gaume & Gosset, 2003; Mendoza *et al.*, 2017), nonparametric regression such as local polynomial (Grantz *et al.*, 2005; Regonda *et al.*, 2006; Bracken *et al.*, 2010; Mendoza *et al.*, 2014), to machine learning techniques

(Callegari *et al.*, 2015; Zhu, Luo, Xu, & Ye, 2019; Wang, Wyatt, & Ochsner, 2023).

The success of the statistical approaches depends on the identification of useful predictors, which can be other hydrological variables or features or large-scale climate indices such as El Niño–Southern Oscillation (ENSO), the Pacific Decadal Oscillation (PDO), the Atlantic Multidecadal Oscillation (AMO), and the Antarctic Oscillation (AAO) among others. For example, in India, strong teleconnection between the Summer Monsoon Rainfall (SMR) and large-scale climate variables such as ENSO and the Indian Ocean Dipole (IOD) has been highly documented (Saji *et al.*, 1999; Curtis *et al.*, 2001; Kumar *et al.*, 2006). However, the influence of ENSO (IOD) on the ISMR was found to be weakened (strengthened) in recent decades (Hrudya, Varikoden, & Vishnu, 2020; Krishnaswamy *et al.*, 2015; Rajagopalan & Molnar, 2012). Several studies have reported strong correlations between annual flow and large-scale climate indices such as AMO, PDO, and ENSO in the Western U.S. (Hidalgo, 2004; Rajagopalan, Cook, Lall, & Ray, 2000; Redmond & Koch, 1991; Timilsena, Piechota, Tootle, & Singh, 2009; Tootle, Piechota, & Singh, 2005). Berri and Flamenco (1999), and Flamenco (2010) found teleconnections between sea surface temperature (SST) regions from previous months and October-March water volume at the Diamante River and Jachal River basins in Argentina. In the case of Chile, Rubio-Álvarez and McPhee (2010) found important correlations between annual and seasonal flow in southern Chile and ENSO, PDO, and AAO for the 1952-2003 period. A positive and significant correlation between the East Central Tropical Pacific SST index (Niño 3.4) and the summer (December-February) seasonal flow at the Aconcagua River

Tecnología y ciencias del agua, ISSN 2007-2422, 16(4), 125-180. DOI: 10.24850/j-tyca-2025-04-04

basin in Central Chile was reported by Martínez, Fernández and Rubio (2012). Recently, Hernandez, Mendoza, Boisier y Ricchetti (2022) confirmed a major influence of ENSO on the hydro climatological variability in rainfall-driven catchments in central and southern Chile (between 28° and 41°S) using streamflow-based signatures, but for snowmelt-driven and mixed regime catchments, the results showed that the way ENSO affects river hydrology depends on the complex interplay between local climate anomalies and catchment-scale characteristics. However, in Chile, there is no evidence of studies of teleconnection between seasonal flow and large-scale climate indices for forecasting purposes (indices from previous seasons or months).

Motivated by the need for skillful seasonal streamflow forecasts in Chile during the dry season (September-March) and the lack of studies on the teleconnections between large-scale climate indices and seasonal flow with predictive purposes, the goal of this study is to identify teleconnections between seasonal flow in the Olivares River basin (ORB) and climatic indices from previous seasons and test if these teleconnections can add predictive skill to a seasonal streamflow forecasting model. To do this, we will conduct a correlation analysis of seasonal streamflow with traditional large-scale climate indices, SST fields, and hydrological variables from the previous seasons (different lead times) to identify potential predictors, and then, we will implement a Multiple Linear Regression (MLR) for seasonal streamflow forecasting considering the potential predictors as inputs.

Tecnología y ciencias del agua, ISSN 2007-2422, 16(4), 125-180. DOI: 10.24850/j-tyca-2025-04-04

Tecnología y Ciencias del Agua
OPEN ACCESS
Check for updates

Materials and methods

Study area and data

This study focuses on the Olivares River basin (ORB), a sub-basin of the Upper Maipo River basin in central Chile (Figure 1a). The ORB has a drainage area of 544 km^2, a south-north orientation, and a length of approximately 50 km. Its drainage area flows into the Maipo River and has an elevation range from around 1 500 masl (outlet) to 6 000 masl (Figure 1b). The upper Maipo River basin has a snowmelt-dominated regime (Figure 1c), i.e., most of the precipitation is accumulated during the winter (June-August) in the form of snow, which melts during the spring and summer seasons (September-March), where the temperature increases (Figure 1d). Consequently, the ORB shows maximum flows during the summer (December to February; Figure 1e).

Tecnología y ciencias del agua, ISSN 2007-2422, 16(4), 125-180. DOI: 10.24850/j-tyca-2025-04-04

Tecnología y Ciencias del Agua
OPEN ACCESS
Check for updates

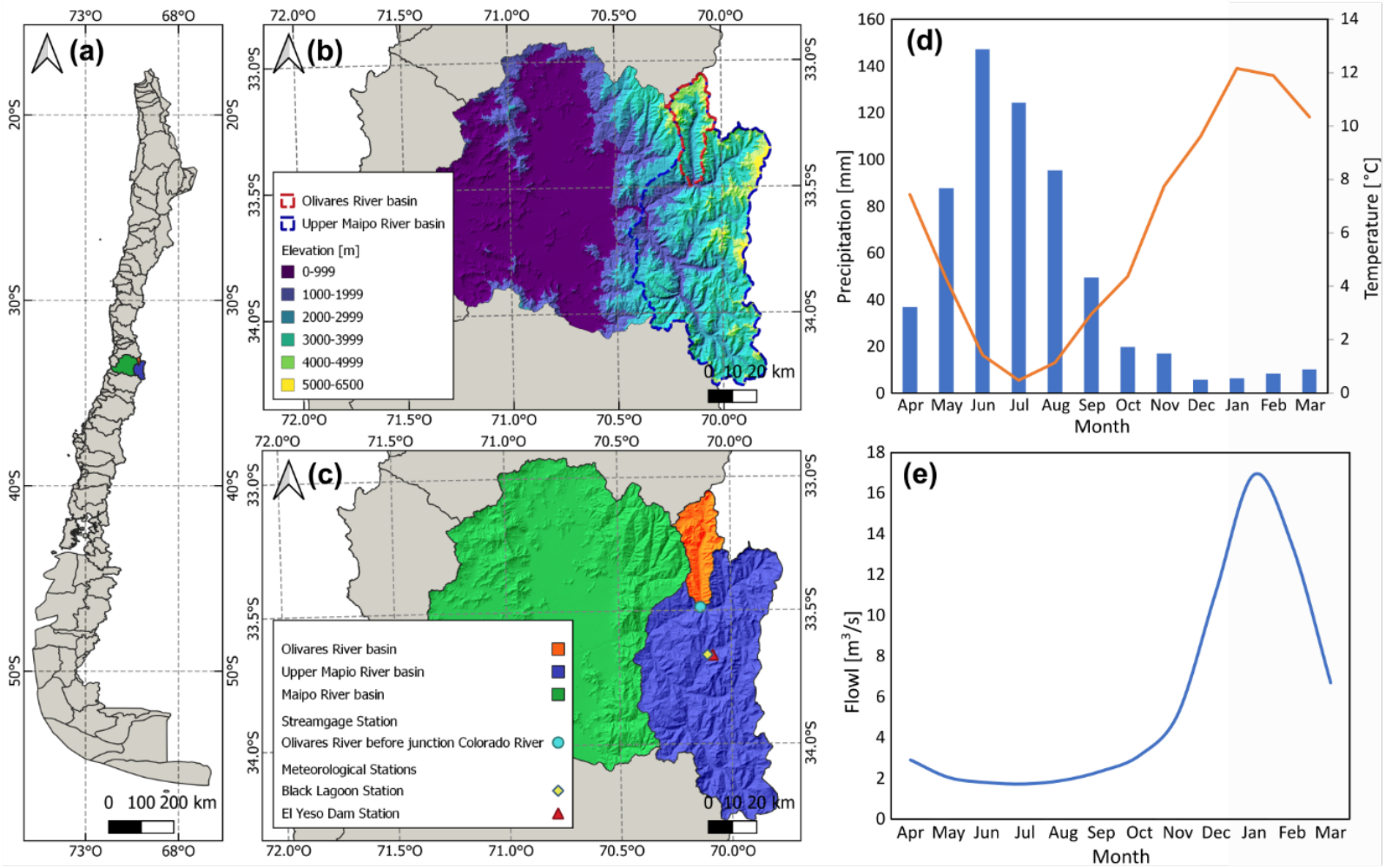

Figure 1. Map illustrating the location of the Olivares River basin (ORB) in central Chile and its hydro-climate regimes. (a) Map of Chile highlighting the location of the ORB. (b) The elevation map of the Maipo River basin. (c) Map of the Maipo River basin and the upper Maipo River basin highlighting the ORB and the location of the stream gage station considered for this study. (d) Average annual climograph for the period 1978-2019. Daily precipitation and temperature records were obtained from the Yeso Embalse and Laguna Negra stations. (e) streamflow monthly variation curves at ORB for the period 1978-2019.

The significance of the Maipo River basin, and all sub-basins within it, resides in that it is one of the most important water supply sources for Santiago, the highest population center in Chile (nearly 40 % of the population) delivering around 70 % of the demand for drinking water and contributing about 90 % of the irrigation demand for this city. In addition, the ORB is vital for hydroelectric power generation in the region.

We obtained the monthly average streamflow data from the Olivares River before the junction with the Colorado River station from the database of the CR2 climate explorer (https://explorador.cr2.cl/) for the period 1978-2019. This station is the terminal gauge of the Olivares River basin (ORB), located at 1500 masl, and 33.4878°S and 70.1367°W (Figure 1c). We selected the ORB station because it has a vast data record due to its strategic location, which does not have long periods of missing data. Then, we computed the seasonal daily average streamflow for the spring (SON, September to November) and summer (DJFM, December to March), which are considered the predictands of the forecasting model implementation.

Regarding meteorological variables, we obtained daily precipitation data from the "El Yeso Embalse" station (Figure 1c) from the database of the CR2 climate explorer (https://explorador.cr2.cl/) for 1978-2019. We selected this station because it is one of the few in the area with a long temporal record without long periods of missing data (no more than 15 % of consecutive days with missing values each month) and its closeness to the ORB station. Gridded global SST anomalies from 1978 to 2019 with 5° spatial resolution were obtained from the International Research Institute (IRI) for Climate and Society at Columbia University (Parker *et*

Tecnología y ciencias del agua, ISSN 2007-2422, 16(4), 125-180. DOI: 10.24850/j-tyca-2025-04-04

al., 1994; Reynolds & Smith, 1994; Kaplan *et al.*, 1998). were obtained monthly 500 mb geopotential height and horizontal and vertical wind components fields from 1978 to 2019 with 5° spatial resolution from the National Centers for Environmental Prediction (NCEP)-National Centers for Atmospheric Research (NCAR) reanalysis dataset (Kalnay *et al.*, 1996; Kistler *et al.*, 2001).

In the case of large-scale climatic indices, we obtained time series of Extreme Eastern Tropical Pacific SST Niño 1+2), East Central Tropical Pacific SST (Niño 3.4), and Antarctic Oscillation (AAO) anomalies from the National Oceanic and Atmospheric Administration (NOAA; https://psl.noaa.gov/data/climateindices/list/) for the same period (1978-2019).

Lead times considered

For this study, we split the dry season into the spring (Sept-Nov) and summer (Dec-March) seasons and consider two lead times (0 and 3-month leads) for each season. By the lead time, we mean the forecast issuance. Figure 2 displays a schematic of the lead times considered for the two seasons. A seasonal spring streamflow forecast with a 0- (3-) month lead corresponds to forecast issuance on September 1 (June 1); thus, the forecast model considers mean seasonal or monthly variables from the previous winter (fall) as predictors (Figure 2a). Similarly, a seasonal summer forecast with a 0- (3-) month lead corresponds to forecast issuance on December 1 (September 1); thus, the forecast model considers the mean seasonal or monthly variables from the previous spring (winter) as predictors (Figure 2b).

Tecnología y Ciencias del Agua
OPEN ACCESS
Check for updates

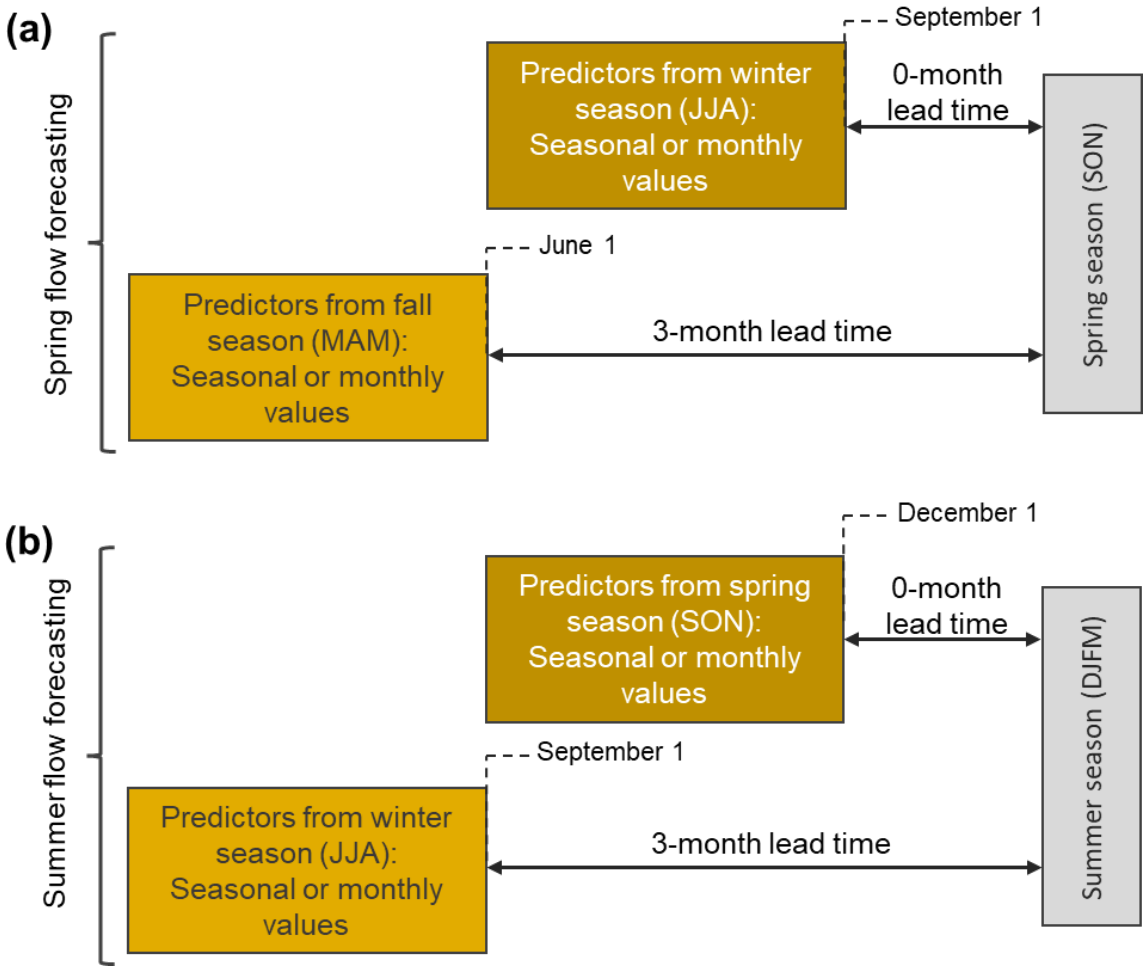

Figure 2. Schematic of the lead times for seasonal spring (a) and summer (b) streamflow forecasts.

Regarding potential predictors, we consider the fall-winter Cumulative Precipitation since the ORB corresponds to a snowmelt-dominated regime basin, and several studies have shown that the snow water equivalent (SWE) accumulated until the beginning of spring is one the most skillful predictors of spring–summer seasonal streamflow across

mountainous regions (e.g., Pagano, 2010; Livneh & Badger, 2020; Ossandón, Brunner, Rajagopalan, & Kleiber, 2022a), and the daily mean streamflow from the month previous to forecast issuance as a potential predictor due to the streamflow persistence reported in previous studies (Bennett et al., 2021; Li, Wang, Bennett, & Robertson, 2015; Li, Wang, Bennett, & Robertson, 2016; Li, Wang, Robertson, & Bennett, 2017). The large-scale climate indices Niño 1+2, Niño 3.4, and AAO are included as potential predictors because the link between these variables and seasonal streamflow in Chilean basins has been demonstrated in past studies (Rubio-Álvarez & McPhee, 2010; Martínez *et al.*, 2012).

In addition, we develop correlation maps between spring (summer) streamflows and Gridded global SST anomalies from the preceding fall and winter (winter and spring) months because there is possible the existence of SST regions of higher teleconnection with seasonal streamflow for the ORB than those predefined regions for the standard ENSO indices.

Methods

Detection of teleconnection of seasonal streamflow with climate and hydrological variables

To assess the correlation (teleconnection) between seasonal streamflow and potential predictors from the previous season (Table 1), we use Spearman's rank correlation coefficient (ρ) (Hollander, Wolfe, & Chicken, 2014). This metric is a nonparametric test that quantifies the behavior similarity between two variables, even though the normality is not verified

for those variables. The Spearman's rank correlation coefficient varies between -1 and 1, with a perfect negative or positive association for 1 or -1, respectively.

Table 1. Description of potential large-scale climate predictors considered for each season and lead time.

Season	**Spring (ρ)**		**Summer (ρ)**	
Potential predictor /Lead time	**0-month**	**3-month**	**0-month**	**-3-month**
AAO	May (-0.34)	May (-0.34)	November (0.33)	May (-0.34)
Niño 3.4	April (-0.15)	April (-0.15)	September (0.13)	August (0.11)
Niño 1+2	February (-0.15)	February (-0.15)	November (0.21)	--

Value in parentheses corresponds to the Spearman's rank correlation.

In the case of the gridded SST anomaly, we aim to identify areas or zones of high positive or negative correlation (ρ) between seasonal streamflow and SST anomaly (HCZ, High Correlation Zones) for each lead time. Next, we calculate new climate indices defined as the spatial mean anomaly of the corresponding SST zone (selected grid cells) and standardize them. In this way, the "new indices" represent areas with a potential predictability for seasonal streamflow.

To understand the physical mechanism behind the teleconnection found for large-scale climate indices and SST anomaly spatial fields, we obtain the composite fields of 500 mb geopotential height and vector winds for the top five wettest years (WY) and driest years (DY). The

wettest and driest were obtained based on the annual precipitation record.

Multiple Linear Regression Model

We implement a multiple linear regression model (MLRM) (Jobson, 1991) for seasonal streamflow forecasting, considering those variables or indices as potential predictors to demonstrate the predictive ability of the teleconnections identified. We use MLRM because of its easy implementation and interpretability, and they have been widely used in forecasting applications at different temporal scales (e.g., Mendoza et al., 2017; Papacharalampous & Tyralis, 2018; Jozaghi *et al.*, 2021). Consider that $Q_j(t)$ for $t=1,\ldots,N$ represents the mean seasonal streamflow (predictand) of the season j at a specific location for the year t. To forecast this variable, we assume that it could be expressed as a linear function of p predictors from k-month lead times as follows

$$Q_j(t) = \beta_o + \sum_{i=1}^{p} \beta_i X_{i,k}(t) + \epsilon \quad (1)$$

Where:

$X_{i,k}(t)$ = denotes the predictor i at the lead time k for the year t

β_o = the intercept

β_i = regression coefficient related to the predictor $X_{i,k}(t)$

ϵ = represents the model error, which is commonly assumed to have a normal probability distribution with mean 0 and standard deviation σ_ϵ

Note that transformed predictors can easily incorporate nonlinear relations between predictand and predictors into MLRM. For example, the power of two of one predictor can be incorporated as a new predictor. Predictors and predictand data are normalized before fitting the MLRM (i.e., z scores are computed using $z=(x-\mu)/\sigma$, where x represents the original variable, and μ and σ represent the mean and standard deviation of x, respectively). Thus, the MLRM is applied in standard-normal space for forecast generation; then, predictands are transformed back to streamflow space (i.e., apply $x=z\sigma+\mu$).

The regression coefficients are estimated using the Maximum Likelihood (ML) approach. We obtained the best MLRM for each lead time as the combination of predictors that resulted in the minimum Akaike Information Criteria (AIC) (Akaike, 1974). The AIC balances the goodness of fit of a model with its complexity, aiming to find the model that best describes the underlying data while penalizing overly complex models. The AIC is defined as:

$$\mathrm{AIC} = -2 \cdot \ln(L) + N_p \tag{2}$$

Where:

L = is the likelihood of the MLRM fitted

N_p= is the number of parameters in the model

The AIC is computed for a suite of candidate models with various combinations of predictors. The model with the minimum AIC is selected to predict the basin's spring or summer maximum streamflow.

Figure 3 provides a general workflow with the sequence of methodological steps for implementing an MLRM for seasonal streamflow forecast at k-month lead time. The methodological steps include the teleconnection analysis, calibration of different MLRM candidates, and the selection of the best MRLR forecast model (set of best predictors).

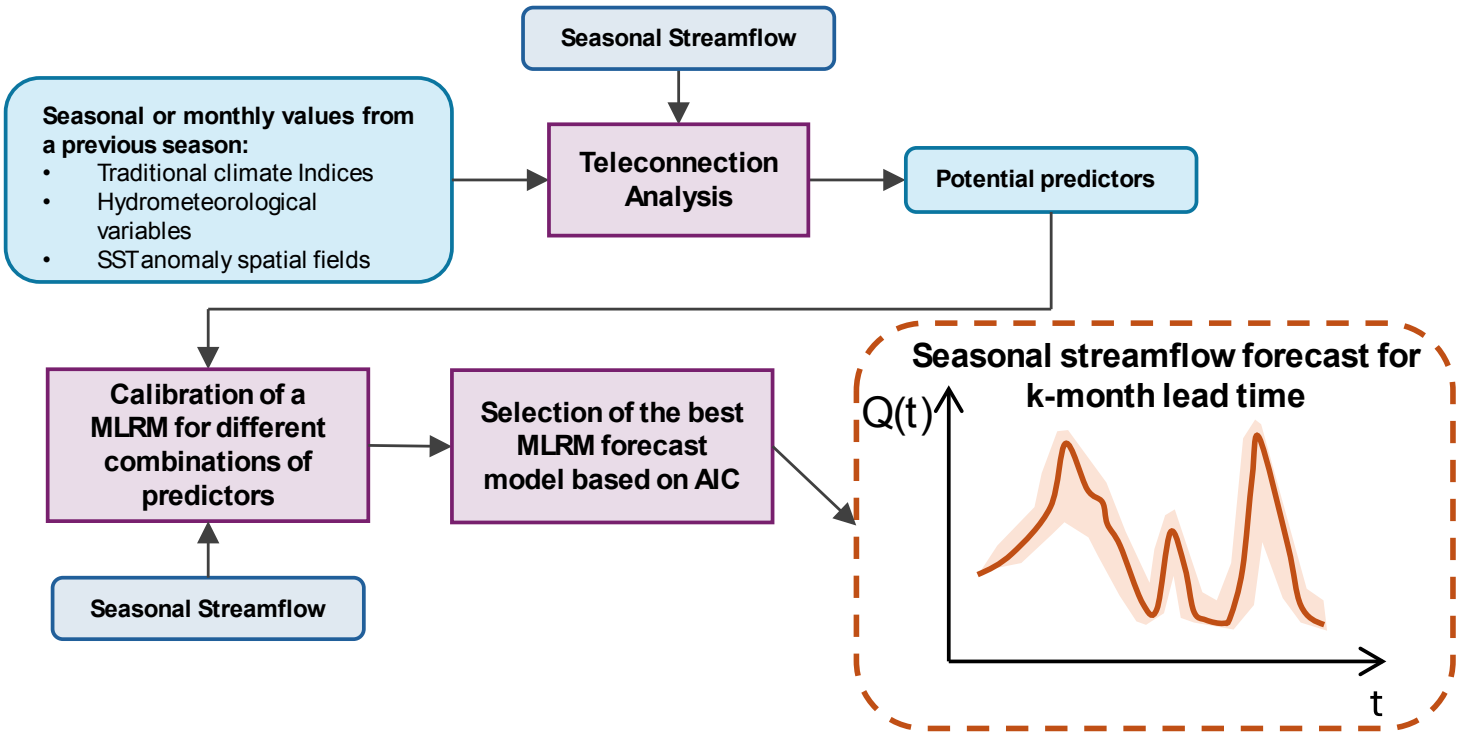

Figure 3. General workflow of implementation of an MLRM for seasonal streamflow forecast at a k-month lead time. Cyan and blue boxes denote the input data (predictors and predictand), purple boxes are the methodological steps, and orange box is the output (seasonal streamflow forecast).

Model cross-validation and verification metrics

To assess the out-of-sample predictability of the model, we perform the leave-1-year-out cross-validation (CV) by dropping one year from the record (1979–2019) and fitting the MLRM using the remaining years, which are also known as the calibration years. The fitted model is applied to provide estimates for the validation year. This cross-validation procedure was repeated N times, where N corresponds to the number of observations. For both calibration and cross-validation, we compute five deterministic metrics to assess their performance. The metrics are the Nash-Sutcliffe efficiency (NSE) (Nash & Sutcliffe, 1970), Pearson's correlation coefficient (R), the percentage bias (BIAS), and the root mean square error (RMSE). In addition, to provide un model uncertainty quantification, we generate streamflow forecast ensembles by simulating 1000 samples of the predicted residuals (ϵ) from a $N(0,\sigma_\epsilon)$ for each year, which are added to the MLRM forecasted value. σ_ϵ is computed from the residuals obtained after fitted the MLRM (Equation (1)). From these ensemble members, we compute the 50 and 99 % confidence intervals, and the continuous rank probability skill score (CRPSS) (Hersbach, 2000; Gneiting & Raftery, 2007). The CRPSS ranges from -∞ to 1. CRPSS 0 indicates that the reference forecast has higher skill than the forecast model, CRPSS 0 implies equal skill, and CRPSS 0 implies that the forecast model has a higher skill, with CRPSS 1 being a perfect score. Here, we considered the climatology as the reference forecast model (i.e., for each year, forecast ensembles are drawn from the historical observed values).

Tecnología y ciencias del agua, ISSN 2007-2422, 16(4), 125-180. DOI: 10.24850/j-tyca-2025-04-04

Results

Teleconnection and correlation analysis

Traditional large-climatic indices

Figure 4 shows the correlation between the seasonal streamflow at the ORB and traditional large-scale climatic indices (AAO, Niño 3.4, and Niño 1+2) for different monthly delays. Regarding spring seasonal streamflow (Figure 4b), significant negative correlations with statistical significance are observed for AAO during January (-8 months, ρ = -0.32), April (-5 months, ρ = -0.33), and May (-4 months, ρ = -0.34). Conversely, other monthly delays, including the synchronous AAO time series (September), exhibit low and non-significant correlations. The correlation coefficients for Niño 1+2 and Niño 3.4 indices range from -0.15 to 0.12 and -0.15 to 0.08 across all monthly delays, indicating weak and non-significant teleconnections. For summer seasonal streamflow, the results reveal predominantly low and non-significant teleconnection values across almost all indices and monthly delays. Notably, AAO demonstrates significant correlations at time delays of -1 month (November, ρ = 0.33), -7 months (May, ρ = -0.34), and -8 months (April, ρ = -0.27).

Tecnología y ciencias del agua, ISSN 2007-2422, 16(4), 125-180. DOI: 10.24850/j-tyca-2025-04-04

Tecnología y Ciencias del Agua
OPEN ACCESS
Check for updates

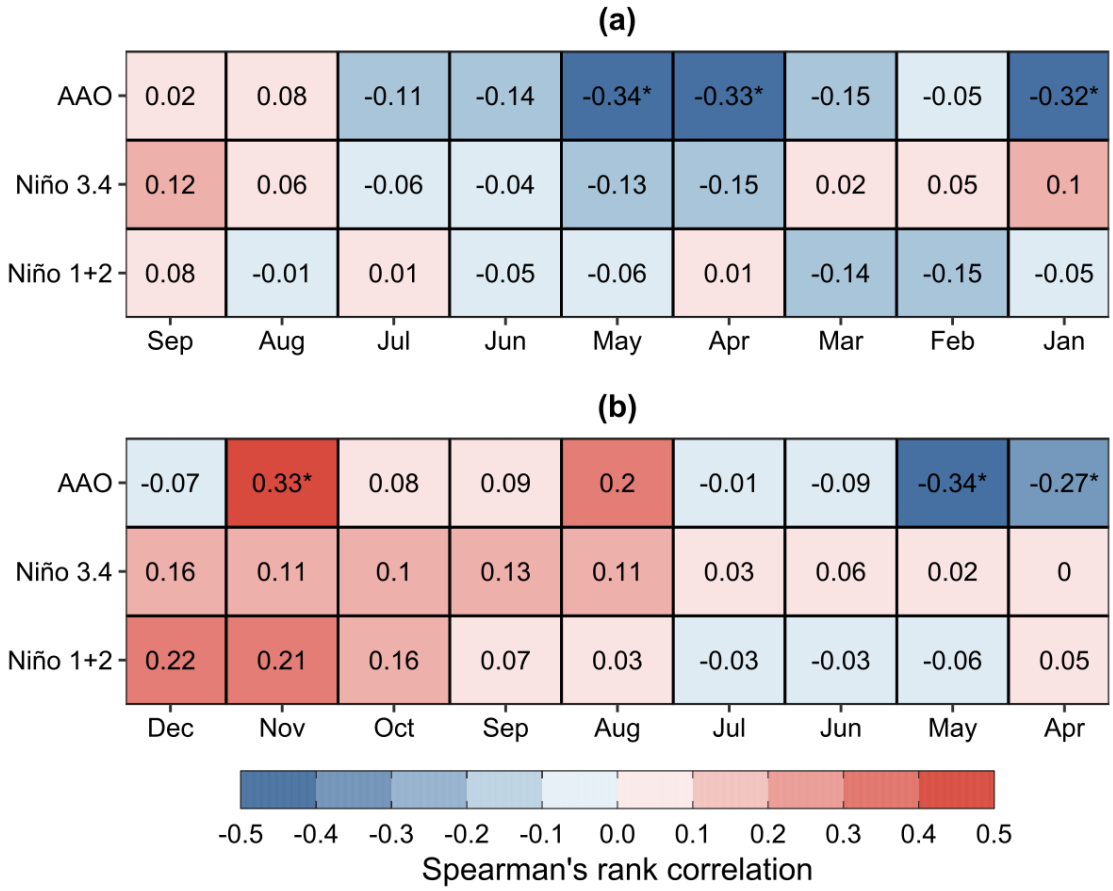

Figure 4. Spearman's rank correlation between seasonal streamflow at the ORB and traditional large-scale climate indices with different monthly delays. (a) Seasonal spring streamflow. (b) Seasonal summer streamflow. Index values for September (December) correspond to a 0-month delay, and values for January (April) correspond to an 8-month delay. * denotes significant correlations at a 90 % confidence level.

Based on these results, for seasonal spring streamflow at the two lead times (0 and 3 months leads) as potential climate predictors, we consider May AAO, April Niño 3.4, and February Niño 1+2. Regarding the seasonal summer streamflow, we include as potential climate predictors Nov AAO and May AAO for 0- and 3-month leads, August and September

Niño 3.4 for 0- and 3-month leads, and November Niño 1+2 for the 0-month lead. We do not include a Niño 1+2 predictor for a 3-month lead due to low correlations for the months before September. Table 1 summarizes the predictors selection for each season and lead time.

Teleconnections with gridded SST anomalies

Figure 5 shows the Spearman rank correlation coefficient between seasonal streamflow (spring and summer) and the three-month average gridded SST anomalies for a 0-month lead time (JJA and SON). Consistent with the findings in Figure 4, both spring and summer seasons exhibit low correlations between seasonal streamflow and the 0-month lead SST anomalies in the Niño 3.4 and Niño 1+2 regions. However, notable zones of high correlation are identified for the two seasons. The region in the Southeast Pacific close to South America (SEPZ; 260-280E, 15-25S) exhibits positive correlations, resembling patterns seen in El Niño events but with improved correlation values. Conversely, the area in the mid-South Pacific (MSPZ; 185-215E, 10-45S) displays negative correlations. This region, closer to Oceania, reflects warm events in the Tropical Pacific or El Niño as negative anomalies. It is worth noting that our area is restricted to the South Pacific region to avoid detecting anecdotal teleconnections that lack physical meaning. For the seasonal spring streamflow, correlation values range between 0.26 and 0.41 in SEPZ, while in MSPZ, they range from -0.66 to -0.25 (Figure 5a). In the case of the seasonal summer streamflow (Figure 5b), correlation values range between 0.20 and 0.34 in SEPZ and between -0.56 and -0.15 in MSPZ. For a 3-month lead time, the same two zones were detected (with a slight correlation reduction, Figure A1).

Tecnología y Ciencias del Agua
OPEN ACCESS
Check for updates

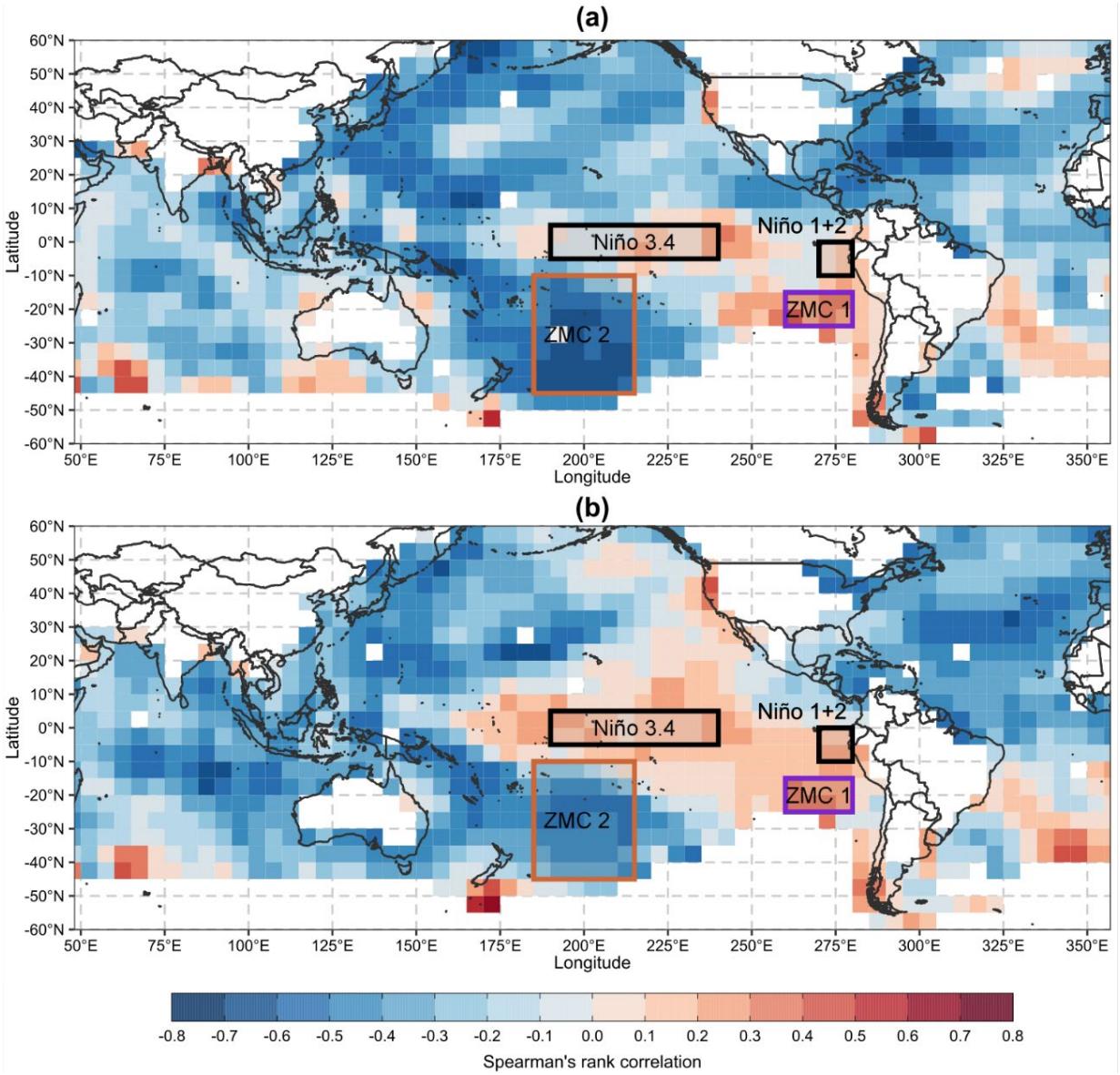

Figure 5. Correlations for a 0-month lead time between (a) seasonal spring streamflow at the ORB and the three-month (June-July-August, JJA) average SST anomalies, (b) seasonal summer streamflow at the ORB and the three-month (September-October-November, SON) average SST anomalies. Black boxes denote zones for traditional climate indices, and purple and yellow are zones of higher correlation -SEPZ and MSPZ, respectively.

For a better understanding of the physical meaning of the SST anomaly and seasonal streamflow teleconnections, Figure 6 displays composite maps of anomalies of geopotential height and vector winds at 500 mb for the top five wettest years (WY, Figure 6a) and driest years (DY, Figure 6b). In these maps, SEPZ and MSPZ exhibit positive and negative values of the 500 mb geopotential height anomaly for DY and WY, respectively. Negative (positive) anomalies correspond to low (high) pressure systems with higher (lower) convergency of humidity compared to climatology. This behavior is consistent with the precipitation pattern of the study area. However, the pattern is weaker for SEPZ, where air mass movement (wind vector fields) convergence for DY and WY is less clear. These results align with the higher SST anomaly teleconnection detected for MSPZ compared to SEPZ.

Tecnología y Ciencias del Agua
OPEN ACCESS
Check for updates

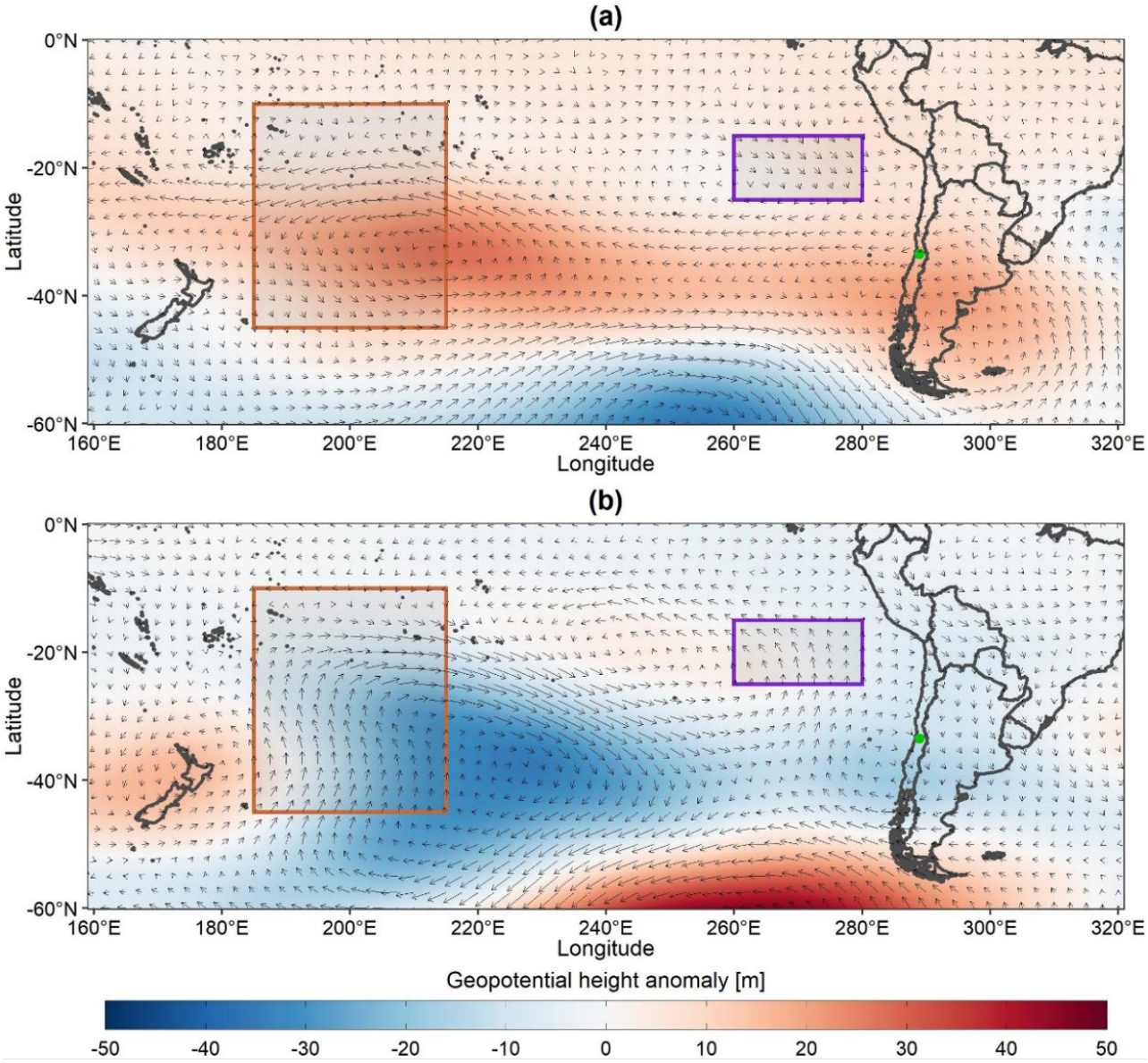

Figure 6. Composite maps of anomalies of geopotential height and vector winds at 500 mb for the top five (a) driest years (DY; 1990, 1996, 1998, 2018, and 2019) and (b) wettest years (WY; 1982, 1987, 2000, 2002, and 2005) and (b). The top five years were obtained based on the annual precipitation record of the study area. The HCZ1 and HCZ2 correspond to the purple and yellow boxes.

Tecnología y ciencias del agua, ISSN 2007-2422, 16(4), 125-180. DOI: 10.24850/j-tyca-2025-04-04

Based on the teleconnection identified, we define two new climate indices, which correspond to spatial aggregate SST anomaly for the two highly correlated zones (for the remainder of the study, we refer to them as SEPZ and MSPZ indices). Table 2 presents Spearman's rank correlation for the SEPZ and MSPZ indices and the spatial mean and standard deviation of Spearman's rank correlation for each zone's mean SST anomaly grid points at different seasons and lead times. The MSPZ exhibits absolute correlation values above 0.5 for both seasons and lead times. However, the standard deviation observed for MSPZ is higher than for SEPZ. This difference may be attributed to the spatial extension of each zone, suggesting potentially greater variability in the correlations within the MSPZ region. In the Multiple Linear Regression Model (MLRM), we will consider the SEPZ and MSPZ indices as potential predictors, respectively.

Tecnología y ciencias del agua, ISSN 2007-2422, 16(4), 125-180. DOI: 10.24850/j-tyca-2025-04-04

Table 2. Spearman's rank correlation for the SEPZ and MSPZ indices and the related spatial mean and standard deviation of the Spearman rank correlation for each zone's mean SST anomaly grid points at different seasons and lead times.

Season	Lead time	Zone	Mean SST anomaly Spearman's rank correlation, ρ		
			Indices	Mean	Standard Deviation
Spring	0-month	SEPZ	0.370	0.321	0.057
	0-month	MSPZ	-0.710*	-0.545	0.122
	3-month	SEPZ	0.344	-0.299	0.044
	3-month	MSPZ	-0.571*	-0.350	0.120
Summer	0-month	SEPZ	0.320	0.290	0.050
	0-month	MSPZ	-0.523*	-0.401	0.140
	3-month	SEPZ	0.322	0.259	0.040
	3-month	MSPZ	-0.541*	-0.421	0.117

* Indicates a significant correlation at a 95 % confidence level.

Hydrometeorological variables

We assess the predictive ability of different hydrometeorological variables in situ by using Spearman's rank correlation coefficient. Table 3 presents correlation values between the seasonal spring and summer streamflow and hydrometeorological variables for 0- and 3-month lead times. These variables include cumulative precipitation (PT) and monthly streamflow for May (August) and August (November) at 0- and 3-month lead times for the seasonal spring (summer) streamflow, respectively. As expected, we observed higher correlations for variables at 0-month lead time than

those at 3-month lead time. Correlations with seasonal streamflow were computed for different monthly streamflows preceding forecast issuance, with consistently higher correlations obtained for the month closest to forecast issuance. This indicates a high flow persistence, consistent with findings reported in previous studies (Bennett *et al.*, 2021; Li *et al.*, 2015; Li *et al.*, 2016; Li *et al.*, 2017).

Table 3. Spearman's rank correlation coefficient between the seasonal spring and summer streamflow and hydrometeorological variables for 0- and 3-month lead times.

Season	Lead time	Hydrometeorological Variable	Spearman's rank correlation, ρ
Spring	0-month	Cumulative precipitation April-August (PT_{AA})	0.502*
	0-month	August monthly flow (Q_{Aug})	0.901*
	3-month	Cumulative precipitation April-May (PT_{AM})	0.253*
	3-month	May monthly flow (Q_{May})	0.695*
Summer	0-month	Cumulative precipitation (PT_{AA})	0.181
	0-month	November monthly flow (Q_{Nov})	0.695*
	3-month	Cumulative precipitation (PT_{AA})	0.181
	3-month	August monthly flow (Q_{Aug})	0.641*

* Indicates a significant correlation at a 95 % confidence level.

Seasonal flow forecasting model

Selection of the best model for each lead time

Different candidate MLRMs (combination of predictors) are calibrated for each season and lead time from 1979 to 2019. The best MLRM for each season and lead time is selected based on the lowest value of AIC (Akaike, 1974). Figure 7 displays the time series of observed seasonal streamflow versus forecasted values from the best MLRM model for each season and lead time, providing visual insight into model performance. Additionally, Table 4 displays the AIC values and other performance metrics for the best models.

Tecnología y Ciencias del Agua
OPEN ACCESS
Check for updates

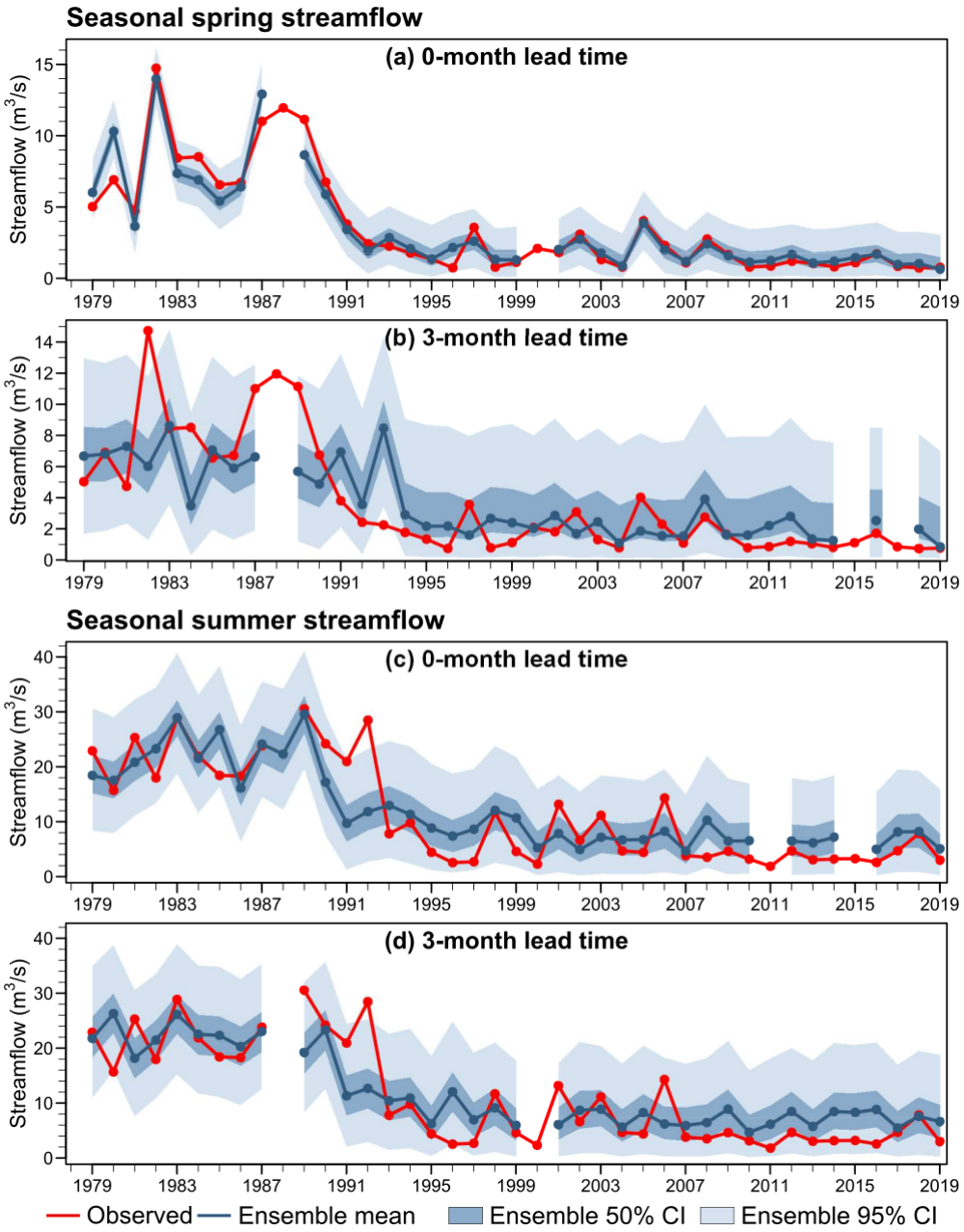

Figure 7. Time series of observed seasonal streamflow and ensembles forecast from the best MLRM calibrated for spring and summer seasons and 0- and 3-month lead times. Red lines denote observed streamflow, blue lines ensemble mean, and blue and light blue bands 50 and 90 % ensemble credible intervals.

Tecnología y ciencias del agua, ISSN 2007-2422, 16(4), 125-180. DOI: 10.24850/j-tyca-2025-04-04

Table 4. Predictors, AIC, and performance metrics values for the best MLRM obtained from the calibration for different seasons and lead times.

Season	Lead time, k	Predictors	AIC	R	BIAS (%)	NSE	RMSE (m^3/s)	CRPSS
Spring	0-month	$Q^2_{Aug}, PT_{AA}, MSPZ$	16.40	0.96	1.10	0.92	0.92	0.71
	3-month	$Q_{May}, MSPZ$	88.57	0.67	3.91	0.45	2.42	0.25
Summer	0-month	$Q_{Nov}, PT_{AA}, MSPZ, AAO$	73.65	0.83	3.81	0.69	5.02	0.46
	3-month	$Q_{Aug}, PT_{AA}, MSPZ, AAO$	81.33	0.80	4.86	0.64	5.36	0.41

For spring, the best forecasting model at a 0-month lead time demonstrates a good fit (Figure 7a), exhibiting high temporal coherence and reduced uncertainty, as indicated by narrow 50 and 90 % credible intervals. Notably, only a few values fall outside the 90 % credible interval, reflecting the model's robustness. Performance metrics further corroborate these attributes, revealing a high correlation (0.96), reduced BIAS and RMSE, and good deterministic and probabilistic skills compared to climatology (NSE = 0.92 and CRPSS = 0.71). However, for 3-month leads, the performance of the best model shows a clear reduction of performance, characterized by low temporal coherence for high flows (before 1990) and increased uncertainty, as evidenced by wider credible intervals (Figure 7b). Performance metrics indicate 30, 51, and 65 % reductions for R, NSE, and CRPSS compared to a 0-month lead.

In the case of the summer streamflow forecasting, there is a decrease in performance compared to the best models for spring at a 0-month lead time. However, both the best models for summer (0 and 3-

month leads) demonstrate similar performances, exhibiting good temporal coherence (correlation coefficients ranging from 0.8 to 0.83), reduced bias (Bias and RMSE ranging from 3.81 to 4.86 % and from 5 to 5.36 m^3/s, respectively), and good deterministic (NSE ~0.4-0.69) and probabilistic (CRPSS ~ 0.41-0.46) skills. This decrease in performance is also reflected by an increase of 50 and 100 % in credible intervals, indicating an increase in uncertainty (Figure 7c and d).

For all lead times, the best models include hydrometeorological and climate predictors from highly correlated SST anomaly zones. A traditional climate index, AAO, is also included as a predictor for summer. Notably, the best model for spring and 0-month leads incorporates a nonlinear transformation of the August mean streamflow (Q^2_{Aug}) as a predictor. This predictor is included due to its reported effectiveness in reducing nonsystematic biases -underestimation (overestimation) of high (low) streamflows (Ossandón, Nanditha, Mendoza, Rajagopalan, & Mishra, et al., 2022b). In the initial implementation, this feature was observed in the calibrated MLRM when we only considered mean streamflow from a previous month as a potential predictor.

Assessment of the Climate Predictors' contribution to forecast models

To assess the contribution of climate predictors to forecast models, Table 5 presents values of AIC and performance metrics for the best MLRM fitted only considering hydrometeorological predictors. It is evident that for all seasons and lead times, including climate variables as predictors, lead to increased performance. The performance improvements are more

Tecnología y ciencias del agua, ISSN 2007-2422, 16(4), 125-180. DOI: 10.24850/j-tyca-2025-04-04

pronounced for the summer season at a 0-month lead time, with a 32 % decrease in BIAS (from 5.58 to 3.81 %) and increases of 13 % (0.72 vs. 0.83), 28 % (0.52 vs. 0.69), and 33 % (0.33 vs. 0.46) in R, NSE, and CRPSS, respectively. Similar performance increases are observed for summer at a 3-month lead when climate variables are included. However, for spring, the increase in performance metrics is relatively lower for both lead times.

Table 5. Predictors, AIC, and performance metrics values for the best MLRM obtained from the calibration for different seasons and lead times using only hydrometeorological predictors.

Season	Lead time, k	Predictors	AIC	R	BIAS (%)	NSE	RMSE (m^3/s)	CRPSS
Spring	0-month	Q_{Aug}^2, PT_{AA}	17.88	0.95	2.54	0.89	1.2	0.66
	3-month	Q_{May}	90.32	0.63	18.69	0.34	3.63	0.23
Summer	0-month	Q_{Nov}, PT_{AA}	76.21	0.72	5.58	0.52	6.34	0.33
	3-month	Q_{Aug}, PT_{AA}	84.23	0.75	6.28	0.55	6.41	0.34

As a complement, Figure 8 displays the time series of the best forecast model with only climate predictors for spring (Figure 8a) and summer (Figure 8b) at a 0-month lead. Contrasting these forecast time series with those presented in Figures 6a and b reveals that climate predictors allow for better capture of the temporal variability and magnitude of observed seasonal streamflow, particularly after 1996 (Figure 7a and Figure 7c). Similar results are observed for 3-month lead times (Figure A2).

Tecnología y Ciencias del Agua
OPEN ACCESS
Check for updates

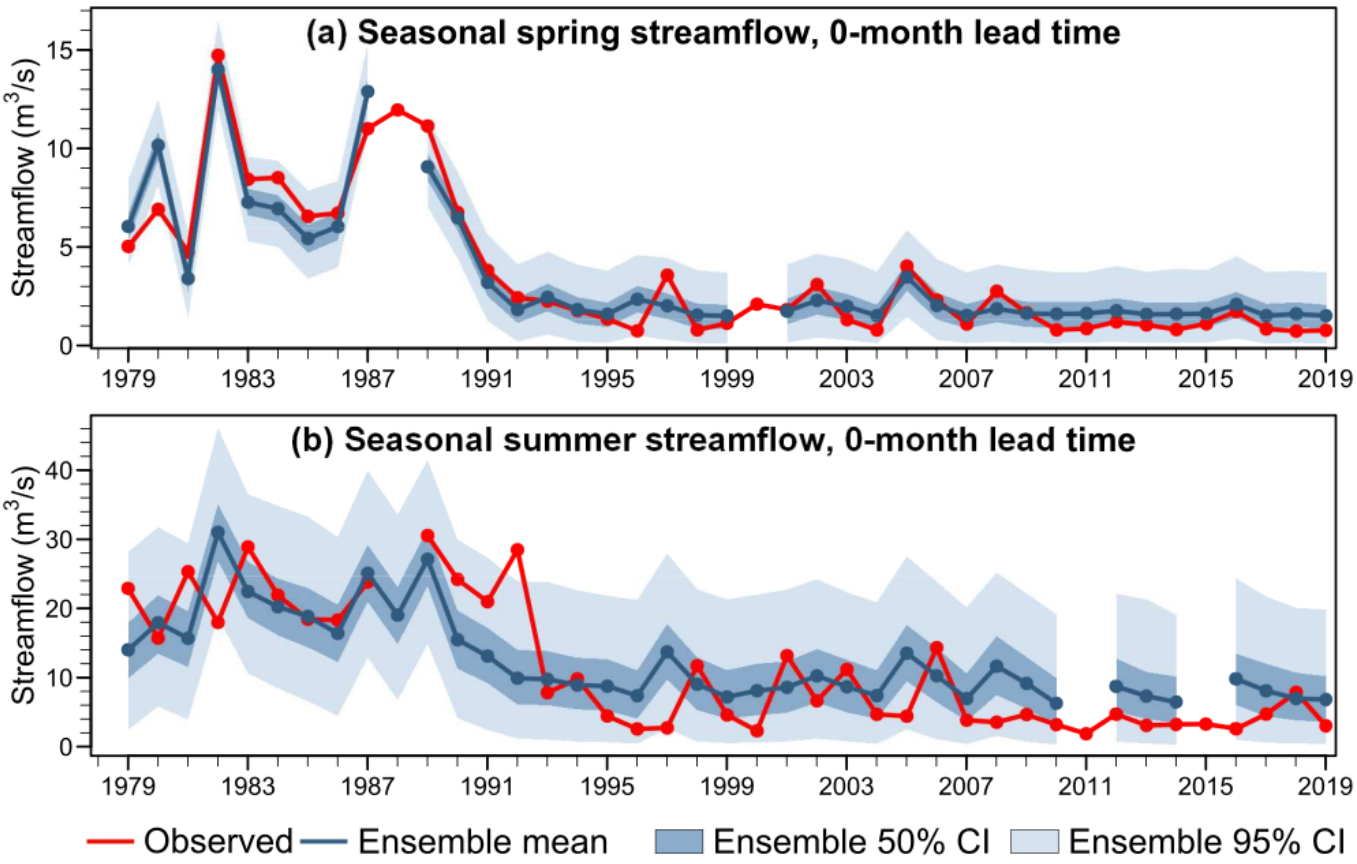

Figure 8. As in Figure 7, but for the best MLRM calibrated only considering hydrometeorological predictors for spring and summer seasons at 0-month lead time.

Cross-validation

Table 6 presents the performance metrics for cross-validated seasonal streamflow for spring and summer at two lead times (0- and 3-month leads). Compared to the calibration results (Table 3), the cross-validation shows a relatively minor reduction in model performance, with correlation coefficients (R) ranging from 0.55 to 0.94 across all seasons and lead

Tecnología y ciencias del agua, ISSN 2007-2422, 16(4), 125-180. DOI: 10.24850/j-tyca-2025-04-04

times. The highest R reduction observed is 18 % for spring streamflow at a 3-month lead time. Similarly, Nash-Sutcliffe Efficiency (NSE) and Continuous Ranked Probability Skill Score (CRPSS) values vary between 0.28 and 0.88 and 0.18 and 0.61, respectively, with the highest skill reduction observed for spring streamflow at a 3-month lead time (38 % for NSE and 28 % for CRPSS). However, despite these reductions, the MLRM models remain more skillful than climatology in all cases. Regarding BIAS and RMSE, there is generally no substantial increase observed for most seasons and lead times, except for spring at a 3-month lead time, which shows a 34 % increase in BIAS and a 30 % increase in RMSE. Nonetheless, the overall performance of the MLRM models in cross-validation remains robust, demonstrating their ability to forecast seasonal streamflow.

Table 6. Performance metrics values for the best MLRM (Table 3) obtained from the cross-validation mode for different seasons and lead times.

Season	Lead time, k	R	BIAS (%)	NSE	RMSE (m^3/s)	CRPSS
Spring	0-month	0.94	1.47	0.88	1.20	0.66
	3-month	0.55	8.70	0.28	2.77	0.18
Summer	0-month	0.78	5.11	0.61	5.33	0.38
	3-month	0.71	4.33	0.50	6.10	0.31

In addition, Figure 9 presents the time series of the cross-validated seasonal streamflow forecast alongside the observed streamflow at 0- and

3-month lead times for both spring and summer seasons. The time series of cross-validated ensemble forecasts corroborate the findings obtained from the performance metrics analysis. For the spring season at a 0-month lead (Figure 9a), the ensemble mean of the cross-validated forecast effectively captures the variability and uncertainty of the data, yielding results similar to those obtained during calibration. However, at a 3-month lead (Figure 9b), as indicated in Table 5, the ensemble mean forecast fails to accurately capture the magnitude of the observed flow for most years, contrasting with the results observed during calibration (Figure 7b). For summer seasonal streamflow, the time series of ensemble forecasts for calibration and cross-validation exhibit similar performance compared to observed streamflows (Figure 9c and Figure 9d).

Tecnología y ciencias del agua, ISSN 2007-2422, 16(4), 125-180. DOI: 10.24850/j-tyca-2025-04-04

Tecnología y Ciencias del Agua
OPEN ACCESS
Check for updates

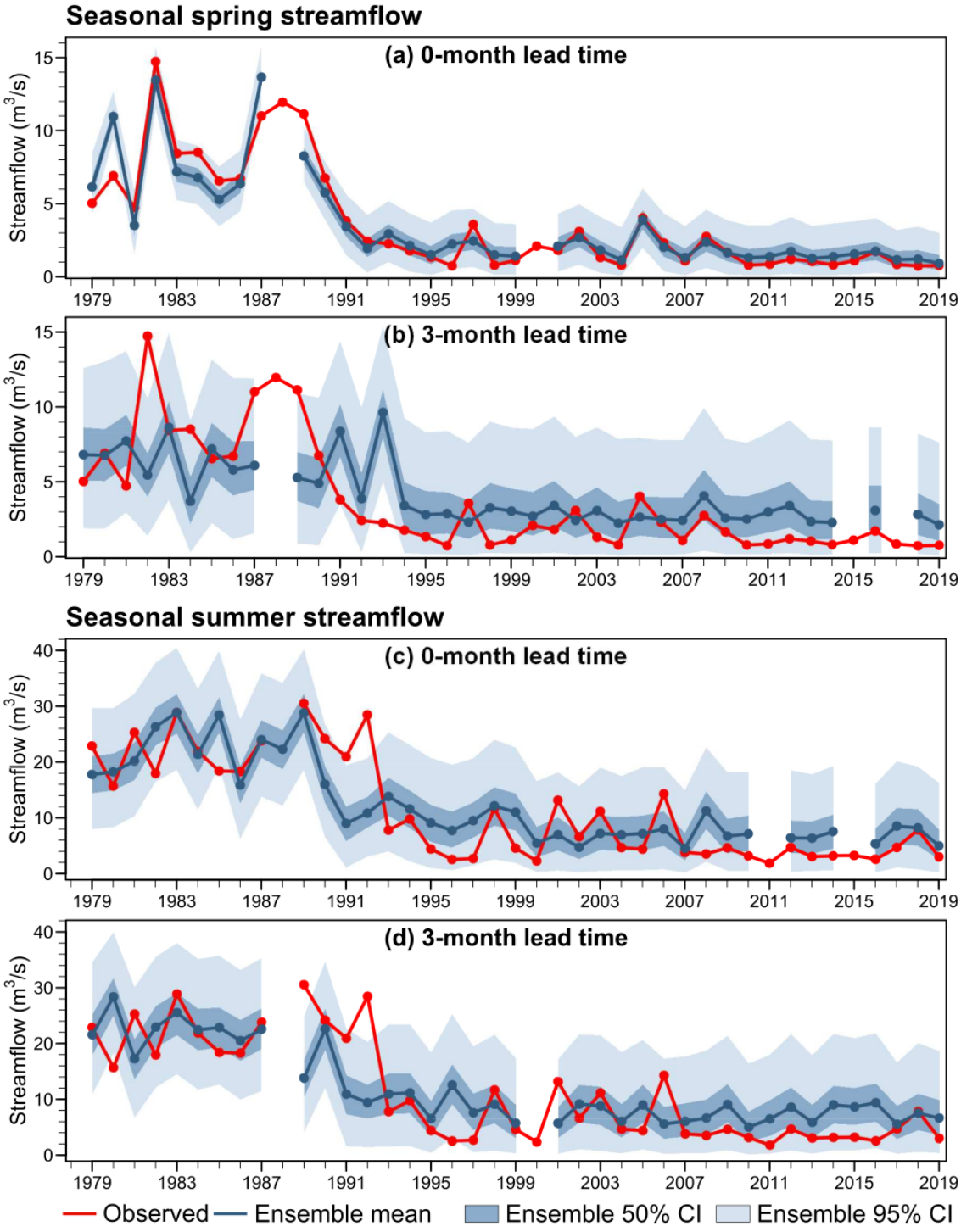

Figure 9. As in Figure 6, but for cross-validation of the best MLRMs for spring and summer seasons at 0- and 3-month lead times.

Tecnología y ciencias del agua, ISSN 2007-2422, 16(4), 125-180. DOI: 10.24850/j-tyca-2025-04-04

Tecnología y Ciencias del Agua
OPEN ACCESS
Check for updates

Summary and discussion

This study presents a teleconnection analysis of the seasonal streamflow at the Olivares River basin (ORB) in central Chile to identify potential predictors for implementing seasonal streamflow forecast models. For the analysis, we consider traditional climate indices (AAO, Niño1+2, and Niño3.4), new indices based on highly correlated zones of sea surface temperature (SST) anomaly spatial fields, and in situ hydrometeorological variables from precedent seasons. We illustrate the potential of the predictors identified by fitting a multiple linear regression model (MLRM) to forecast seasonal streamflow (spring and summer) for two lead times (0- and 3-month leads). We assess the predictive performance of the MLRM forecasts using a leave-1-year-out cross-validation (LOOCV) approach and different performance metrics (R, BIAS, RMSE, NSE, and CRPSS).

The teleconnection analysis for the traditional indices (AAO, Niño1+2, and Niño3.4) showed only significant correlations with low values (below 0.4 in magnitude) for a few time delays. These results are different from those reported in previous studies (Rubio-Álvarez & McPhee, 2010; Martínez et al., 2012). Still, the differences can be related to the temporal extension of the data considered in these studies (up to 2003), which did not include information from the Central Chile Mega Drought (2010–2018) (Garreaud *et al.*, 2020). Another possible explanation for this results discrepancy could be a weakening of the teleconnection between hydrological variables and large-scale traditional indices during the last decade, as was reported for India (Hrudya *et al.*,

2020; Krishnaswamy *et al.*, 2015; Rajagopalan & Molnar, 2012). In the ORB, the weakening of teleconnection can also be attributed to the abrupt change in the seasonal flow regime after 1992 (Figure 7). This change in flow regime was caused by the beginning of the Alfalfal hydroelectric power plant operation, which is located upstream of the ORB gauge.

We defined two new climate indices (SEPZ and MSPZ) based on highly correlated SST anomaly spatial field zones for the ORB to overcome the teleconnection lack with traditional large-scale climate indices. These indices correspond to spatial aggregate SST anomaly for the respective zones. The physical connection of these regions of the Pacific Ocean with ORB was supported by the composite fields of 500 mb geopotential height. The absolute value of correlation for these indices ranges from 0.32 to 0.71.

As hydrometeorological predictors, we considered cumulative precipitation during the wet season and monthly flow from the season's last month before the forecast issuance of each lead time. Monthly flows from the last month of the previous season showed a high and significant correlation with seasonal streamflow for all seasons and lead times (values above 0.64). These results reveal an increased persistence of streamflow processes in the basin, an appealing feature exploited by other authors in the implementation of forecasting and simulating models in different regions of the world (Bennett *et al.*, 2021; Li *et al.*, 2015; Li *et al.*, 2016; Li *et al.*, 2017).

The best MLRM selection for each season and lead time confirms the high persistence of the streamflow processes on the ORB. This is because the monthly flow from the previous season was selected as a predictor for all the models. The MSPZ index was included as a predictor of the MLRM

for all seasons and lead times, except spring at 3-month leads, highlighting the utility of teleconnection analysis for the area of interest. The added predictive value of including these climate indices in the forecasting models reveals increases of up 13, 28, and 33 % in R, NSE, and CRPSS for the summer season. The best forecasting MLRM for seasonal spring streamflow at 3-month leads has the lowest performance between best models from all seasons and lead times, which is reflected by the inability of the ensemble mean forecast to capture high flows before 1992.

The results of the MLRM predicting out-of-sample (Cross-validation) are encouraging since they show a low reduction in performance compared to the calibration, providing a skillful seasonal flow forecast for spring at a 0-month lead and summer season up to 3-month leads.

Although the results of the MLRM forecasting are encouraging, they cannot be considered conclusive since we did not test the model adequacy (e.g., the normality assumption of the data). More complex forecasting models can be tested in future work considering the predictors identified here to find an adequate forecasting model. For example, Generalized Linear models (GLM, normality of the data is not required) or nonstationary probabilistic models such as General additive models for location, scale, and shape (GAMLSS) (Rigby, Stasinopoulos, & Lane, 2005) can be implemented. In addition, implementing Bayesian approaches can include uncertainty quantification of models' parameters. Moreover, the teleconnection analysis and forecasting models implemented in this study have the potential to be expanded to other basins in Chile and different regions globally. However, the success of the

forecasting model will depend on how powerful climatic teleconnections can be detected.

Finally, this research contributes to identifying potential skillful covariates for their use in implementing forecasting tools to develop robust water management strategies to tackle water scarcity, conditions expected to increase due to global and anthropogenic climate change in this highly populated region of Chile.

Acknowledgments

This research was funded by the ANID Fondecyt Initiation Project 11220482.

Tecnología y ciencias del agua, ISSN 2007-2422, 16(4), 125-180. DOI: 10.24850/j-tyca-2025-04-04

Tecnología y Ciencias del Agua
OPEN ACCESS
Check for updates

Appendix A

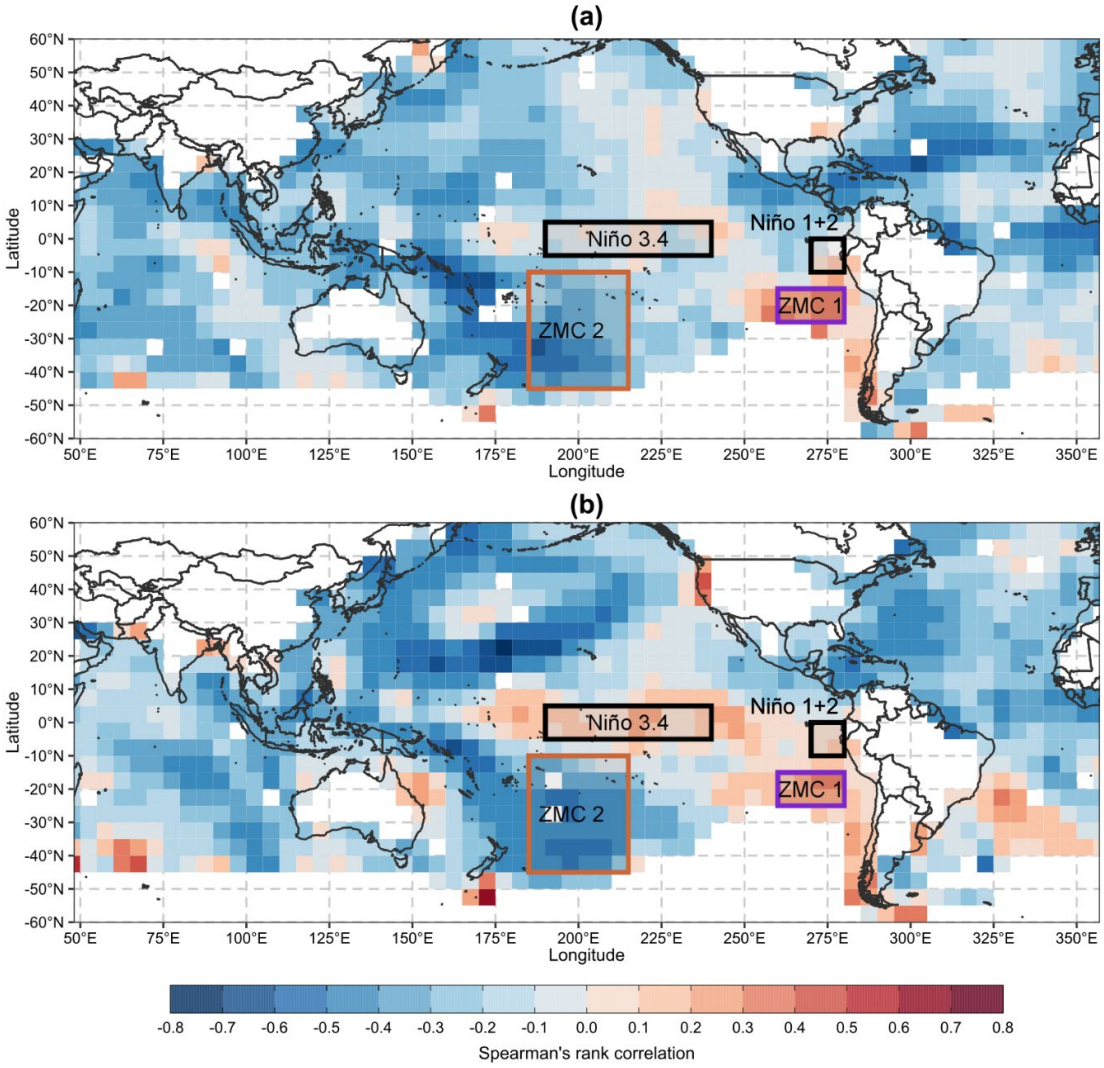

Figure A1. Correlations for a 3-month lead time between (a) seasonal spring streamflow at the ORB and the three-month (June-July-August, JJA) average SST anomalies, (b) seasonal summer streamflow at the ORB and the three-month (September-October-November, SON) average SST anomalies. Black boxes denote zones for traditional climate indices, and purple and yellow are zones of higher correlation -SEPZ and MSPZ, respectively.

Tecnología y ciencias del agua, ISSN 2007-2422, 16(4), 125-180. DOI: 10.24850/j-tyca-2025-04-04

Tecnología y Ciencias del Agua
OPEN ACCESS
Check for updates

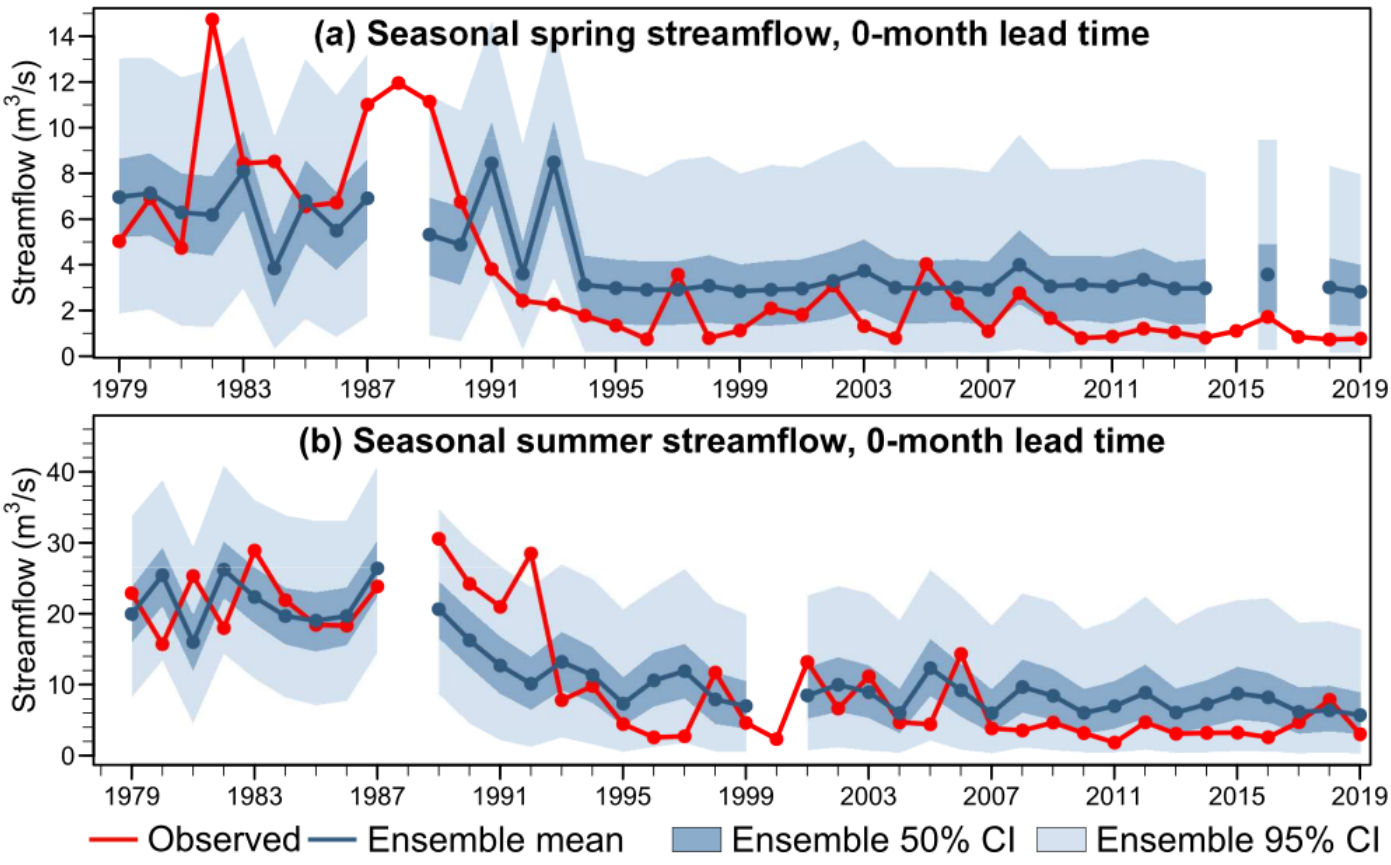

Figure A2. Time series of observed seasonal streamflow and ensembles forecast from the best MLRM calibrated only considering hydrometeorological predictors for spring and summer seasons and a 3-month lead time. Red lines denote observed streamflow, blue lines ensemble mean, and blue and light blue bands 50 and 90 % ensemble credible intervals.

Tecnología y ciencias del agua, ISSN 2007-2422, 16(4), 125-180. DOI: 10.24850/j-tyca-2025-04-04

References

Akaike, H. (1974). A new look at the statistical model identification. *IEEE Transactions on Automatic Control*, 19(6), 716-723. DOI: 10.1109/TAC.1974.1100705

Araya, D., Mendoza, P. A., Muñoz-Castro, E., & McPhee, J. (2023). Towards robust seasonal streamflow forecasts in mountainous catchments: Impact of calibration metric selection in hydrological modeling. *Hydrology and Earth System Sciences*, 27(24), 4385-4408. DOI: 10.5194/HESS-27-4385-2023

Arnal, L., Cloke, H. L., Stephens, E., Wetterhall, F., Prudhomme, C., Neumann, J., Krzeminski, B., & Pappenberger, F. (2018). Skilful seasonal forecasts of streamflow over Europe*? Hydrology and Earth System Sciences*, 22(4), 2057-2072. DOI: 10.5194/HESS-22-2057-2018

Bennett, J. C., Wang, Q. J., Li, M., Robertson, D. E., & Schepen, A. (2016). Reliable long-range ensemble streamflow forecasts: Combining calibrated climate forecasts with a conceptual runoff model and a staged error model. *Water Resources Research*, 52(10), 8238-8259. DOI: 10.1002/2016WR019193

Bennett, J. C., Wang, Q. J., Robertson, D. E., Bridgart, R., Lerat, J., Li, M., & Michael, K. (2021). An error model for long-range ensemble forecasts of ephemeral rivers. *Advances in Water Resources*, 151, 103891. DOI: 10.1016/J.ADVWATRES.2021.103891

Berri, G. J., & Flamenco, E. A. (1999). Seasonal volume forecast of the Diamante River, Argentina, based on El Niño observations and predictions. *Water Resources Research*, 35(12), 3803-3810. DOI: 10.1029/1999WR900260

Block, P., & Rajagopalan, B. (2009). Statistical-dynamical approach for streamflow modeling at Malakal, Sudan, on the White Nile River. *Journal of Hydrologic Engineering*, 14(2), 185-196. DOI: 10.1061/(asce)1084-0699(2009)14:2(185)

Bracken, C., Rajagopalan, B., & Prairie, J. (2010). A multisite seasonal ensemble streamflow forecasting technique. *Water Resources Research*, 46(3), W03532. DOI: 10.1029/2009WR007965

Bradley, A. A., Habib, M., & Schwartz, S. S. (2015). Climate index weighting of ensemble streamflow forecasts using a simple Bayesian approach. *Water Resources Research*, 51(9), 7382-7400. DOI: 10.1002/2014WR016811

Callegari, M., Mazzoli, P., de Gregorio, L., Notarnicola, C., Pasolli, L., Petitta, M., & Pistocchi, A. (2015). Seasonal river discharge forecasting using support vector regression: A case study in the Italian Alps. *Water*, 7(5), 2494-2515. DOI: 10.3390/W7052494

Ćeron, J. P., Tanguy, G., Franchistéguy, L., Martin, E., Regimbeau, F., & Vidal, J. P. (2010). Hydrological seasonal forecast over France: Feasibility and prospects. *Atmospheric Science Letters*, 11(2), 78-82. DOI: 10.1002/ASL.256

Chiew, F. H. S., Zhou, S. L., & McMahon, T. A. (2003). Use of seasonal streamflow forecasts in water resources management. *Journal of Hydrology*, 270(1-2), 135-144. DOI: 10.1016/S0022-1694(02)00292-5

Clark, M. P., & Hay, L. E. (2004). Use of medium-range numerical weather prediction model output to produce forecasts of streamflow. *Journal of Hydrometeorology*, 5(1), 15-32. DOI: 10.1175/1525-7541(2004)005<0015:UOMNWP>2.0.CO;2

CONIC-BF. (2023). *Pronóstico de deshielo cuencas ríos Aconcagua, Maipo, Rapel, Tinguiririca, Maule, Laja y Bío-Bío*. Recovered from https://www.coordinador.cl/mercados/documentos/pronostico-centralizado-de-generacion-y-demanda-2/pronostico-de-deshielo/

Curtis, S., Adler, R., Huffman, G., Nelkin, E., & Bolvin, D. (2001). Evolution of tropical and extratropical precipitation anomalies during the 1997-1999 ENSO cycle. *International Journal of Climatology*, 21(8), 961-971. DOI: 10.1002/JOC.643

DGA, Dirección General de Aguas. (2022). *Pronóstico de caudales de deshielo periodo septiembre/2022-marzo/2023. SDT No. 44, 26*. Recovered from https://snia.mop.gob.cl/repositoriodga/handle/20.500.13000/125978

Flamenco, E. A. (2010). *Pronóstico estacional de caudales en la cuenca del río Jachal*. XXII Congreso Nacional del Agua. Recovered from https://www.researchgate.net/publication/266904038_Pronostico_estacional_de_caudales_en_la_cuenca_del_rio_Jachal

Garreaud, R. D., Alvarez-Garreton, C., Barichivich, J., Pablo-Boisier, J., Christie, D., Galleguillos, M., LeQuesne, C., McPhee, J., & Zambrano-Bigiarini. M. (2017). The 2010-2015 megadrought in central Chile: Impacts on regional hydroclimate and vegetation. *Hydrology and Earth System Sciences*, 21(12), 6307–6327. DOI: 10.5194/HESS-21-6307-2017

Garreaud, R. D., Boisier, J. P., Rondanelli, R., Montecinos, A., Sepúlveda, H. H., & Veloso-Aguila, D. (2020). The Central Chile mega drought (2010-2018): A climate dynamics perspective. *International Journal of Climatology*, 40(1), 421-439. DOI: 10.1002/JOC.6219

Gaume, E., & Gosset, R. (2003). Over-parameterisation, a major obstacle to the use of artificial neural networks in hydrology? *Hydrology and Earth System Sciences*, 7(5), 693-706. DOI: 10.5194/hess-7-693-2003

Gneiting, T., & Raftery, A. E. (2007). Strictly proper scoring rules, prediction, and estimation. *Journal of the American Statistical Association*, 102(477), 359-378. DOI: 10.1198/016214506000001437

González-Reyes, Á. (2016). Ocurrencia de eventos de sequías en la ciudad de Santiago de Chile desde mediados del siglo XIX. *Revista de Geografía Norte Grande*, (64), 21-32. DOI: 10.4067/S0718-34022016000200003

Grantz, K., Rajagopalan, B., Clark, M., & Zagona, E. (2005). A technique for incorporating large-scale climate information in basin-scale ensemble streamflow forecasts. *Water Resources Research*, 41(10), 10410. DOI: 10.1029/2004WR003467

Hernandez, D., Mendoza, P. A., Boisier, J. P., & Ricchetti, F. (2022). Hydrologic sensitivities and ENSO variability across hydrological regimes in Central Chile (28°-41°S). *Water Resources Research*, 58(9), e2021WR031860. DOI: 10.1029/2021WR031860

Hersbach, H. (2000). Decomposition of the continuous ranked probability score for ensemble prediction systems. *Weather and Forecasting*, 15(5), 559-570. DOI: 10.1175/1520-0434(2000)015<0559:DOTCRP>2.0.CO;2

Hidalgo, H. G. (2004). Climate precursors of multidecadal drought variability in the western United States. *Water Resources Research*, 40(12), 1-10. DOI: 10.1029/2004WR003350

Hollander, M., Wolfe, D. A., & Chicken, E. (2014). *Nonparametric statistical methods* (3rd ed.). New York, USA: John Wiley & Sons. DOI: 10.1002/9781119196037

Hrudya, P. H., Varikoden, H., & Vishnu, R. (2020). A review on the Indian summer monsoon rainfall, variability and its association with ENSO and IOD. *Meteorology and Atmospheric Physics*, 133(1), 1-14. DOI: 10.1007/S00703-020-00734-5

IPCC, The Intergovernmental Panel on Climate Change. (2022). Climate change 2022: Impacts, adaptation and vulnerability. In: Pörtner, H.-O., Roberts, D. C., Tignor, M., Poloczanska, E., Mintenbeck, K. Alegría, A. *et al*. (eds.). *Working Group II Contribution to the Sixth Assessment Report of the Intergovernmental Panel on Climate Change*. Cambridge, UK and New York, NY, USA: Cambridge University Press. DOI: 10.1017/9781009325844

Jobson, J. D. (1991). *Multiple linear regression*. DOI: 10.1007/978-1-4612-0955-3_4

Jozaghi, A., Shen, H., Ghazvinian, M., Seo, D. J., Zhang, Y., Welles, E., & Reed, S. (2021). Multi-model streamflow prediction using conditional bias-penalized multiple linear regression. *Stochastic Environmental Research and Risk Assessment*, 35(11), 2355-2373. DOI: 10.1007/s00477-021-02048-3

Kalnay, E., Kanamitsu, M., Kistler, R., Collins, W., Deaven, D., & Gandin, L. (1996). The NCEP / NCAR 40-year reanalysis project. *Bulletin of the American Meteorological Society*, 77(3), 437-472. DOI: 10.1175/1520-0477(1996)077<0437:TNYRP>2.0.CO;2

Kaplan, A., Cane, M. A., Kushnir, Y., Clement, A. C., Blumenthal, M. B., & Rajagopalan, B. (1998). Analyses of global sea surface temperature 1856-1991. *Journal of Geophysical Research: Oceans*, 103(C9), 18567-18589. DOI: 10.1029/97JC01736

Kistler, R., Kalnay, E., Collins, W., Saha, S., White, G., Woollen, J., Chelliah, M., Ebisuzaki, W., Kanamitsu, M., Kousky, V., van den Dool, H., Jenne, R., & Fiorino, M. (2001). The NCEP-NCAR 50-year reanalysis: Monthly means CD-ROM and documentation. *Bulletin of the American Meteorological Society*, 82(2), 247-267. DOI: 10.1175/1520-0477(2001)082<0247:TNNYRM>2.3.CO;2

Kompor, W., Yoshikawa, S., & Kanae, S. (2020). Use of seasonal streamflow forecasts for flood mitigation with adaptive reservoir operation: A case study of the Chao Phraya River Basin, Thailand, in 2011. *Water*, 12(11), 3210. DOI: 10.3390/W12113210

Krishnaswamy, J., Vaidyanathan, S., Rajagopalan, B., Bonell, M., Sankaran, M., Bhalla, R. S., & Badiger, S. (2015). Non-stationary and non-linear influence of ENSO and Indian Ocean Dipole on the variability of Indian monsoon rainfall and extreme rain events. *Climate Dynamics*, 45(1-2), 175-184. DOI: 10.1007/S00382-014-2288-0

Kumar, K. K., Rajagopalan, B., Hoerling, M., Bates, G., & Cane, M. (2006). Unraveling the mystery of Indian monsoon failure during El Niño. *Science*, 314(5796), 115-119. DOI: 10.1126/SCIENCE.1131152

Li, M., Wang, Q. J., Bennett, J. C., & Robertson, D. E. (2015). A strategy to overcome adverse effects of autoregressive updating of streamflow forecasts. *Hydrology and Earth System Sciences*, 19(1), 1–15. DOI: 10.5194/HESS-19-1-2015

Li, M., Wang, Q. J., Bennett, J. C., & Robertson, D. E. (2016). Error reduction and representation in stages (ERRIS) in hydrological modelling for ensemble streamflow forecasting. *Hydrology and Earth System Sciences*, 20(9), 3561-3579. DOI: 10.5194/HESS-20-3561-2016

Li, M., Wang, Q. J., Robertson, D. E., & Bennett, J. C. (2017). Improved error modelling for streamflow forecasting at hourly time steps by splitting hydrographs into rising and falling limbs. *Journal of Hydrology*, 555, 586-599. DOI: 10.1016/J.JHYDROL.2017.10.057

Livneh, B., & Badger, A. M. (2020). Drought less predictable under declining future snowpack. *Nature Climate Change*, 10(5), 452-458. DOI: 10.1038/s41558-020-0754-8

Martínez, C., Fernández, A., & Rubio, P. (2012). Caudales y variabilidad climática en una cuenca de latitudes medias en Sudamérica: río Aconcagua, Chile Central (33oS). *Boletín de la Asociación de Geógrafos Españoles*, (58), 227-248. DOI: 10.21138/bage.2066

Mendoza, P. A., Rajagopalan, B., Clark, M. P., Cortés, G., & McPhee, J. (2014). A robust multimodel framework for ensemble seasonal hydroclimatic forecasts. *Water Resources Research*, 50(7), 6030-6052. DOI: 10.1002/2014WR015426

Mendoza, P. A., Wood, A. W., Clark, E., Rothwell, E., Clark, M. P., Nijssen, B., Brekke, L. D., & Arnold, J. R. (2017). An intercomparison of approaches for improving operational seasonal streamflow forecasts. *Hydrology and Earth System Sciences*, 21(7), 3915-3935. DOI: 10.5194/hess-21-3915-2017

Nash, J. E., & Sutcliffe, J. V. (1970). River flow forecasting through conceptual models part I - A discussion of principles. *Journal of Hydrology*, 10(3), 282-290. DOI: 10.1016/0022-1694(70)90255-6

Ossandón, Á., Brunner, M. I., Rajagopalan, B., & Kleiber, W. (2022a). A space–time Bayesian hierarchical modeling framework for projection of seasonal maximum streamflow. *Hydrology and Earth System Sciences*, 26(1), 149-166. DOI: 10.5194/HESS-26-149-2022

Ossandón, Á., Nanditha, J. S., Mendoza, P. A., Rajagopalan, B., & Mishra, V. (2022b). A bayesian hierarchical framework for postprocessing daily streamflow simulations across a river network. *Journal of Hydrometeorology*, 23(6), 947-963. DOI: 10.1175/JHM-D-21-0167.1

Pagano, T. C. (2010). Soils, snow and streamflow. *Nature Geoscience*, 3(9), 591-592. DOI: 10.1038/ngeo948

Paiva, R. C. D., Collischonn, W., Bonnet, M. P., De Gonçalves, L. G. G., Calmant, S., Getirana, A., & Santos-Da-Silva, J. (2013). Assimilating in situ and radar altimetry data into a large-scale hydrologic-hydrodynamic model for streamflow forecast in the Amazon. *Hydrology and Earth System Sciences*, 17(7), 2929-2946. DOI: 10.5194/hess-17-2929-2013

Papacharalampous, G. A., & Tyralis, H. (2018). Evaluation of random forests and prophet for daily streamflow forecasting. *Advances in Geosciences*, 45, 201-208. DOI: 10.5194/adgeo-45-201-2018

Parker, D. E., Jones, P. D., Folland, C. K., & Bevan, A. (1994). Interdecadal changes of surface temperature since the late nineteenth century. *Journal of Geophysical Research: Atmospheres*, 99(D7), 14373-14399. DOI: 10.1029/94JD00548

Petry, I., Fan, F. M., Siqueira, V. A., Collishonn, W., Cauduro-Dias-de-Paiva, R. Quedi, E., Gama, C., Silveira, R., Freitas, C., & Paranhos, C. S. A. (2023). Seasonal streamflow forecasting in South America's largest rivers. *Journal of Hydrology: Regional Studies*, 49(August). DOI: 10.1016/j.ejrh.2023.101487

Rajagopalan, B., Cook, E., Lall, U., & Ray, B. K. (2000). Spatiotemporal variability of ENSO and SST teleconnections to summer drought over the United States during the twentieth century. *Journal of Climate*, 13(24), 4244-4255. DOI: 10.1175/1520-0442(2000)013<4244:SVOEAS>2.0.CO;2

Rajagopalan, B., & Molnar, P. (2012). Pacific Ocean sea-surface temperature variability and predictability of rainfall in the early and late parts of the Indian summer monsoon season. *Climate Dynamics*, 39(6), 1543-1557. DOI: 10.1007/S00382-011-1194-Y

Redmond, K. T., & Koch, R. W. (1991). Surface climate and streamflow variability in the Western United States and their relationship to large-scale circulation indices. *Water Resources Research*, 27(9), 2381-2399. DOI: 10.1029/91WR00690

Regonda, S. K., Rajagopalan, B., Clark, M., & Zagona, E. (2006). A multimodel ensemble forecast framework: Application to spring seasonal flows in the Gunnison River Basin. *Water Resources Research*, 42(9), 9404. DOI: 10.1029/2005WR004653

Reynolds, R. W., & Smith, T. M. (1994). Improved global sea surface temperature analyses using optimum interpolation. *Journal of Climate*, 7(6), 929-948. DOI: 10.1175/1520-0442(1994)007<0929:IGSSTA>2.0.CO;2

Rigby, R. A., Stasinopoulos, D. M., & Lane, P. W. (2005). Generalized additive models for location, scale and shape. *Journal of the Royal Statistical Society: Series C* (Applied Statistics), 54(3), 507-554. DOI: 10.1111/J.1467-9876.2005.00510.X

Rubio-Álvarez, E., & McPhee, J. (2010). Patterns of spatial and temporal variability in streamflow records in south central Chile in the period 1952-2003. *Water Resources Research*, 46(5), 1-16. DOI: 10.1029/2009WR007982

Saji, N. H., Goswami, B. N., Vinayachandran, P. N., & Yamagata, T. (1999). A dipole mode in the tropical Indian Ocean. *Nature*, 401, 6751, 401(6751), 360-363. DOI: 10.1038/43854

Serrano-Notivoli, R., Tejedor, E., Sarricolea, P., Meseguer-Ruiz, O., Vuille, M., Fuentealba, M., & De Luis, M. (2021). Hydroclimatic variability in Santiago (Chile) since the 16th century. *International Journal of Climatology*, 41(S1), E2015-E2030. DOI: 10.1002/JOC.6828

Singla, S., Céron, J. P., Martin, E., Regimbeau, F., Déqué, M., Habets, F., & Vidal, J. P. (2012). Predictability of soil moisture and river flows over France for the spring season. *Hydrology and Earth System Sciences*, 16(1), 201-216. DOI: 10.5194/HESS-16-201-2012

Sutanto, S. J., Wetterhall, F., & Van Lanen, H. A. J. (2020). Hydrological drought forecasts outperform meteorological drought forecasts. *Environmental Research Letters*, 15(8), 084010. DOI: 10.1088/1748-9326/AB8B13

Sutanto, S. J., & Van Lanen, H. A. J. (2021). Streamflow drought: Implication of drought definitions and its application for drought forecasting. *Hydrology and Earth System Sciences*, 25(7), 3991-4023. DOI: 10.5194/hess-25-3991-2021

Timilsena, J., Piechota, T., Tootle, G., & Singh, A. (2009). Associations of interdecadal/interannual climate variability and long-term colorado river basin streamflow. *Journal of Hydrology*, 365(3-4), 289-301. DOI: 10.1016/j.jhydrol.2008.11.035

Tootle, G. A., Piechota, T. C., & Singh, A. (2005). Coupled oceanic-atmospheric variability and U.S. streamflow. *Water Resources Research*, 41(12), 1-11. DOI: 10.1029/2005WR004381

Vicuña, S., Gironás, J., Meza, F. J., Cruzat, M. L., Jelinek, M., Bustos, E., Poblete, D., & Bambach, N. (2013). Exploring possible connections between hydrological extreme events and climate change in central south Chile. *Hydrological Sciences Journal*, 58(8), 1598–1619. DOI: 10.1080/02626667.2013.840380

Wang, M., Wyatt, B. M., & Ochsner, T. E. (2023). Accurate statistical seasonal streamflow forecasts developed by incorporating remote sensing soil moisture and terrestrial water storage anomaly information. *Journal of Hydrology*, 626, 130154. DOI: 10.1016/J.JHYDROL.2023.130154

Wijayarathne, D. B., & Coulibaly, P. (2020). Identification of hydrological models for operational flood forecasting in St. John's, Newfoundland, Canada. *Journal of Hydrology: Regional Studies*, 27. DOI: 10.1016/j.ejrh.2019.100646

Wilcox, A. C., Escauriaza, C., Agredano, R., Mignot, E., Zuazo, V., Otárola, S., Castro, L., Gironás, J., Cienfuegos, R., & Mao, L. (2016). An integrated analysis of the March 2015 Atacama floods. *Geophysical Research Letters*, 43(15), 8035-8043. DOI: 10.1002/2016GL069751

Winsemius, H. C., Aerts, J. C. J. H., Van Beek, L. P. H., Bierkens, M. F. P., Bouwman, A., Jongman, B., Kwadijk, J. C. J., Ligtvoet, W., Lucas, P. L., van Vuuren, D. P., & Ward, P. J. (2016). Global drivers of future river flood risk. *Nature Climate Change*, 6(4), 381-385. DOI: 10.1038/nclimate2893

Wood, A. W., Kumar, A., & Lettenmaier, D. P. (2005). A retrospective assessment of National Centers for Environmental Prediction climate model–based ensemble hydrologic forecasting in the western United States. *Journal of Geophysical Research: Atmospheres*, 110(D4), 1-16. DOI: 10.1029/2004JD004508

Yuan, X., Wood, E. F., & Ma, Z. (2015). A review on climate-model-based seasonal hydrologic forecasting: physical understanding and system development. *Wiley Interdisciplinary Reviews: Water*, 2(5), 523-536. DOI: 10.1002/wat2.1088

Zhu, S., Luo, X., Xu, Z., & Ye, L. (2019). Seasonal streamflow forecasts using mixture-kernel GPR and advanced methods of input variable selection. *Hydrology Research*, 50(1), 200-214. DOI: 10.2166/NH.2018.023